Evaluation of Soil Disturbance due to Sonic Drilling using Instrumentation and Cone Penetration Test Measurements

By

KEVIN CALDWELL GREEN

THESIS

Submitted in partial satisfaction of the requirements for the degree of

MASTER OF SCIENCE

in

Civil and Environmental Engineering

in the

OFFICE OF GRADUATE STUDIES

of the

UNIVERSITY OF CALIFORNIA

DAVIS

Approved:

_____

Jason T. DeJong, Chair

_____

Daniel W. Wilson

_____

Alejandro Martinez Vela

Committee in Charge
2021

Evaluation of Soil Disturbance due to Sonic Drilling using Instrumentation and Cone Penetration Test Measurements

ABSTRACT

Sonic drilling is an efficient and versatile drilling technique used to continuously core soils and soft rock, and it is increasingly used for geotechnical site characterization. During sonic drilling, the sonic head and attached drill string are vibrated to advance the drill string into the subsurface. These vibrations are transmitted to and propagated through the surrounding soil, causing some amount of disturbance to the soil. However, the magnitude of disturbance as a function of the zone of influence (radial and vertical distance) and soil type has not yet been quantified. This thesis presents the results of two field studies that quantify the sonic induced soil disturbance with an array of installed instrumentation. In addition, as an indicator of the possible disturbance to in-situ tests or soil sampling below the bit, changes in baseline measured CPT parameters are evaluated when a CPT sounding is performed into soils immediately below the sonic casing.

ACKNOWLEDGEMENTS

I am immensely grateful for the guidance, mentorship and friendship given to me by my advisor and thesis chair, Professor Jason T. DeJong. I am continually amazed by his insight, ardor and fastidiousness in furthering the field of geotechnical engineering. I would also like to thank Dr. Daniel Wilson, whose patience with my progress at the CGM and knowledge of everything needed to interpret digital data has proved deeply useful and enlightening. Finally, I would like to thank Professor Alejandro Martinez Vela for his willingness to serve on my committee.

This work would not have been possible without the help of everyone who participated in the field studies, including Pete Bowen and the field crew at ConeTec, Inc. in Salt Lake City, as well as Zak Janus, Mark Knoelle and the field crew at Terra Sonic International in Marietta, Ohio. I am deeply indebted to all of them for their time, energy and effort spent to produce two the field investigations essential to this thesis. Furthermore, I would like to thank Jamie Sharp of ConeTec Inc. and Mike Parkinson of Mud Bay Drilling for providing support and guidance regarding field implementation and interpretation of the field results.

I would also like to thank my colleagues at the UC Davis Center for Geotechnical Modeling: Anatoliy Ganchenko, Tom Khonke, and Chad Justice, as well as the development team at Adara, Ltd.: Ron Dolling, Ong Siau-Hwa and Shawn Liu. Their experience and expertise, which reaches far beyond the realm of geotechnical engineering, was requisite for creating, testing and utilizing the specialized equipment used in this study.

Finally, I would like to thank ConeTec, Inc. for their funding support of this research program.

TABLE OF CONTENTS

LIST OF TABLES

LIST OF FIGURES

INTRODUCTION

Sonic Drilling Background

Sonic drilling is a technique that uses vibrations to advance drill casing through the subsurface. Sonic drilling is typically faster than other drilling methods and results in significantly less waste because soil cuttings are, in most cases, displaced rather than brought to the surface through augers or fluid circulation. One of the main benefits of sonic drilling is its ability to continuously core through many types of formations and retrieve continuous cores, offering an uninterrupted profile of the subsurface. Similar to a rotary boring, SPT sampling, thin-walled tube sampling, or in-situ testing may be deployed from the base of a sonic borehole.

Mechanics of Sonic Drilling

Sonic drill rigs consist of two main vibratory components that are used to advance the core barrel and drill casing into the subsurface: the sonic head and the drill string, as shown in Figure 1. The sonic head contains two hydraulically powered counter-rotating eccentric masses, which spin in opposing circular motions such that the vertical motions of the counter-rotating oscillators are synchronous, while the horizontal motions are equal and opposite. Superposition of the two counter-rotating oscillators cancels out the horizontal components and creates a purely uniaxial vertical vibration. This uniaxial vibration of the sonic head is transmitted to the drill string and bit to advance the system through the subsurface, thus transmitting vibrations to the surrounding soil. The sonic head and drill string are mechanically isolated from the rest of the rig by an air cushion, which prevents transmission of waves generated by the sonic head through rig components other than the drill string. While the vibrations induced by the sonic head propagate down the drill string, the air cushion dampens out motions that would otherwise be transferred to other rig components.

In addition to supplying vibrations, the sonic head will rotate the drill string as well as apply a hydraulically powered downward pressure. The vibration frequency and intensity, down pressure and rotational speed are all controlled by the operator. Typical frequencies of sonic drill rigs range from to 50 to 200 Hz (Lucon 2013) and rotation rates are generally around 1.5 rotations per second.

Optimal energy transmission from the sonic head to string to soil occurs when the drill string and soil are in a resonance condition, known as the "system resonance" (Massarsch et al 2021); therefore, sonic drill rig operators seek to achieve resonance (or a condition close to resonance) of the drill string to optimize penetration rates. The frequency at which resonance is achieved depends on the length and material of the drill pipe (typically steel), as well as the stiffnesses of the soils in contact with the drill string along the shaft and at the tip. For an idealized, one-dimensional, freely vibrating steel pipe (i.e. not in contact with any material), the resonance frequency is given by the following equation:

$$f_n = \frac{c}{2l} \qquad [1]$$

where f_n is the natural frequency at which resonance occurs, c is the speed of mechanical deformation of the material, and l is the pipe length. For sonic drilling, c is approximately 5,030 m/s, and l is the length of the drill string. f_n refers to the fundamental frequency, although overtones and undertones of this frequency (multiples of two and one-half, respectively) will also theoretically achieve resonance. Because the system resonance includes the stiffness and the damping effects of the soil, as well as drill strings with joints at the drill rod breaks, the resonance

frequency achieved during sonic drilling is less than this theoretical value. However, the frequency-length relationship of equation [1] still holds during sonic drilling: as the length of drill string is increased (i.e. deeper penetration), the system resonance frequency decreases. Sonic drill rigs have a limited frequency range, generally 50 to 200 Hz, therefore a driller may operate the rig at an overtone or an undertone of the fundamental system resonance frequency. Traditionally, the resonance frequency is found during penetration by qualitative operator observations. As a result of this, sonic drilling tends to be operator dependent.

The mechanism by which sonic drilling is advanced is not fully understood. Some research suggests that sonic vibrations fluidize the soil surrounding the drill string up to a few mm away (Barrow 1994), allowing for less frictional shaft resistance. Other researchers (Massasrch et al. 2021) have suggested that the vertical oscillations during penetration create horizontal oscillations, which reduced horizontal stress. Horizontal oscillations are indeed induced during penetration (as shown later in the paper and in Massarsch et al. (2021), indicating that cyclic decreases in horizontal stress may play a role in increased penetration rates. Beneath the tip of the drill, soils are easily displaced around the bit by the vibrations. In rock formations where purely vibrational displacement is not readily achieved, the bit can pulverize the rock to allow displacement.

Sonic Drilling and Disturbance

The magnitude of disturbance that sonic drilling induces to the surrounding soil is unknown, and therefore there is concern that the measurements obtained from standard tests for geotechnical investigations (e.g. SPT, CPT, vane) may be compromised to some extent when used with sonic drilling. The mode and quantification of this disturbance, in terms of changes in soil fabric, pore pressure, stress, or volume, is not well-established or studied. ASTM D1586 states

that there are "concerns, undocumented by research….that the extreme dynamic loading and vibrations could disturb some soils such as sands and soft clays past the seating interval," and this disturbance could influence the SPT N value or CPT q_c measurement. Wentz and Dickenson (2013) monitored pore pressure response due to sonic drilling and SPT sampling at a silty sand/sandy silt site. Pore pressure measurements as close as 0.3 m away laterally from the drill string showed that a maximum pore pressure ratio, defined as the maximum excess pore pressure Δu divided by the effective vertical stress σ'_v, of 0.13 was induced by sonic vibrations. Additionally, the generated pore pressures from a sonic run dissipated well before SPTs below the sonic casing could be performed, as shown in Figure 2. The study also compared SPT N values obtained directly below sonic and mud rotary borings and found no systematic bias between the two methods (although it was noted that the sample size was too small to make generalized conclusions). This indicates that for this study, pore pressure increase as close as 0.3 m away from the borehole did not significantly result in soil disturbance that directly affected SPT N values.

Watkins et al. (2020) performed a similar field study at a sandy site where sonic, direct push and rotary boreholes were advanced, and then SPT tests were performed at the base of the boreholes. They found that differences in SPT N values obtained beneath sonic and rotary boreholes were not statistically significant within the inherent variability of SPT test results.

Objective of this Study

The primary objective of this study was to improve the body of research on sonic drilling and its effects on soil disturbance by obtaining data during and after sonic drilling. To achieve this, field testing and data acquisition was performed at two sites: Phase I in Salt Lake City, Utah

(December 2020), and Phase II in Marietta, Ohio (June 2021). The two main bodies of data acquired during these field tests to accomplish this study's objective include the following:

1. In-situ soil motions close to the sonic borehole, measured during sonic drilling using custom push-in probe instrumentation, termed "SonicWands."
2. A comparison of (a) baseline CPT measurements (acquired before sonic drilling) and (b) CPT measurements from soundings advanced directly from the bottom of a sonic borehole (referred to as "post-sonic CPTs").

INSTRUMENTATION

A primary component of the field testing was to measure in-situ ground motions induced by the sonic drill rig during penetration. Ten push-in probes, termed "SonicWands", were developed by ConeTec Inc. and the University of California, Davis, to measure these motions. Each SonicWand consisted of a sensor module housed in a 44 mm diameter, 429 mm long stainless steel rod with a 60 degree cone tip that could be coupled to conventional CPT rods for insertion into the subsurface. For Phase I (Salt Lake City), the sensor module in each SonicWand included seven transducer channels: three uni-directional geophones (one each oriented in the vertical and two horizontal axes), a pore pressure transducer, two tiltmeter accelerometers (one each oriented in the two horizontal axes, offset 45 degrees from the geophone orientation), and a temperature sensor. The geophones were connected to an amplifier that increased the measured voltage within the SonicWand by a factor of 838. For Phase II (Marietta), the three geophones were replaced with three uni-directional 200g-range MEMS accelerometers (one each oriented in the vertical and two horizontal axes), which were amplified by a factor of 3. The geophones were replaced in Phase II due to geophone saturation during Phase I field testing, although ultimately the replacement accelerometers had too large a range to record high-quality data, as discussed in more detail later.

The sensor module within each SonicWand was connected to a 45-meter cable, which connected to a custom National Instruments based data acquisition system (DAS). The DAS was used to simultaneously sample up to seven channels from eight SonicWands (maximum of 56 unique records at a time) during testing at sampling rates ranging from 1024 to 4096 Hz. A schematic of the Phase I SonicWand is shown in Figure 3, and a manufactured SonicWand is shown in Figure 4. Note that Figure 3 shows a resistance transducer; this was actually a

temperature gauge. During field testing, the SonicWands were advanced into the subsurface at select depths to record soil motions during drilling.

In addition to the "downhole" sensors housed in the SonicWand, an "uphole" light sensor was used during testing to measure the rotational speed of the drill string. The light sensor consisted of a transducer that would simultaneously shine a laser and record a voltage spike when the laser was reflected back at the sensor. During field testing, the sensor was attached to a stainless steel L-bracket that was bolted to the tub of the drill rig, which is affixed on the exterior of the air cushion, shown in Figure 5. A reflector was attached to the drill shaft such that the sensor would record one voltage spike every full shaft rotation. It was determined after the field tests that the sampling frequency (i.e. once per revolution) was too low to produce high-resolution rotational speed data.

Sensor Calibration

The geophones and ADXL377 accelerometers used in the study were tested in the laboratory to generate calibration factors to convert measured voltages into engineering units. The geophones used in Phase I were calibrated after Phase I testing, and the ADXL377 accelerometers used in Phase II were calibrated prior to and after Phase II testing.

To calibrate the geophones and the accelerometers, the SonicWands were placed on the arm of the 1-meter-radius centrifuge at the University of California, Davis, which is capable of horizontal shaking (i.e. perpendicular to the arm axis). Each SonicWand was mounted in a custom triangular aluminum frame designed to couple the SonicWand rigidly to the shaker. The SonicWand was mounted such that the axis of the sensor to be calibrated was oriented in the direction of the shaking. To test the X and Y oriented sensors, the SonicWand was mounted

vertically, and to test the Z oriented sensors the SonicWand was mounted horizontally. A control ICP accelerometer with a known calibration factor was then attached to a plastic collar mounted on the SonicWand in the same direction of the shaking. Figures 6a and 6b show the centrifuge arm, the mounting of the SonicWand into the frame in the X/Y and Z directions, respectively, and the collar with the ICP accelerometer.

To test the geophones used in Phase I, a 100-cycle sinusoid with an amplitude of approximately 0.1g was applied to the shaker at 50, 100 and 150 Hz. These frequencies were selected in order to evaluate the range of frequencies that the geophones would likely experience during the field test. At each frequency, the recorded geophone signal was differentiated and then compared to the control accelerometer signal to generate a best-fit line. The slope of the best-fit line between the two datasets was considered the calibration factor. Although the manufacturer datasheet claims that the frequency response of the geophones is slightly non-linear within the 50 to 150 Hz range, a constant calibration factor of 0.11 m/s/V was selected for the geophones based on the results of the laboratory calibration. The ADXL337 accelerometers used in Phase II were tested in a similar manner using a sweep sinusoid beginning at 50 Hz, increasing by 10 Hz up to 150 Hz. The sinusoid had an amplitude of approximately 20g, with 10 cycles per frequency. The calibration testing indicated that the accelerometer is essentially non-linear within this frequency range (confirmed by manufacturer's specification sheet), and a calibration factor of 42 g/V was selected. Figures 7 and 8 show a sample data recording of the ADXL337 accelerometer and the ICP accelerometer in the Z direction at 150 Hz. In Figure 7, the signals have been offset to center around zero, and the y axis shows recorded units (voltage for the ADXL337 and g's for the ICP). In Figure 8, both signals have been normalized such that the peak-to-peak amplitude of each is 2 units. Figure 9 shows the ADXL337 data plotted against the ICP and the resulting best-fit linear

regression line, the slope of which is the calibration factor. The calibration factor for this particular recording was 42.9 g/V.

The uphole light sensor simply recorded 10 volts when triggered, and produced no voltage otherwise. Therefore, no calibration was needed.

FIELD TESTING

To evaluate the disturbance of sonic drilling and its effect on in-situ measurements, two field studies were conducted, including a Phase I in Salt Lake City, Utah, and a Phase II in Marietta, Ohio. The data collected from the field studies included the following:

1. In-situ soil motions close to the sonic borehole, measured during sonic drilling using custom push-in probe instrumentation, termed "SonicWands."
2. A comparison of (a) baseline CPT measurements (acquired before sonic drilling) and (b) CPT measurements from soundings advanced directly from the bottom of a sonic borehole (referred to as "post-sonic CPTs").

Salt Lake City, Utah

Phase I of the field testing program was conducted in ConeTec, Inc.'s yard in Salt Lake City, Utah and included the advancement of seven CPTs to establish baseline subsurface conditions at the site, nine SonicWands to measure soil motions during sonic drilling, and four sonic boreholes with post-sonic CPTs pushed through the borehole bottom to compare to baseline values. Baseline CPTs were pushed from November 23 to 30, 2020, and the remainder of field testing was completed from December 11 to 14, 2020.

Site and Subsurface Conditions

Subsurface conditions at the Salt Lake City site were evaluated based on a desktop review of geologic conditions and measured parameters from the seven baseline CPTs, which were advanced to a depth of about 15 m. The site is located in the alluvial valley between the Wasatch Mountains and the Great Salt Lake, and consists of about 0.5 m of surficial fill underlain by

Holocene-aged sediments, including young, deltaic distributary-channel clays, silts and sands. The groundwater level at the site is approximately 1.5 m below the ground surface. Although a goal of the study was to test the effects of sonic drilling in different soil types, the site contained few relatively homogenous layers. Layers of interest were selected based on the overall composition of the layer, although some degree of heterogeneity was present in each. Depths targeted for the field study included a soft clay and silt layer from about 5 to 8.5 m, a thin layer of interbedded low-stiffness silt and sand from about 9 to 11 m, and a layer of dense sand from about 13.5 m to the termination of the CPTs at a depth of 15 m. The CPT results for one of the baseline CPTs (CPT7) is shown in Figure 10a and a compilation of results from all seven CPTs is shown in Figure 10b.

Testing

Upon completion of the baseline CPTs, the remainder of field testing commenced. A high-level overview of the process is summarized as such:

1. Advance nine SonicWands to target depths of 6, 10 and 14 m with a truck mounted CPT rig
2. Drill four sonic borings to a depth of 15 m, stopping at 7.9 and 10.9 m to advance a 2 m long CPT sounding from the bottom of the borehole.

During insertion, the SonicWands were coupled to conventional CPT rods, and were pushed into the subsurface using a truck-mounted CPT rig. All SonicWands were oriented in the same direction, such that the X geophone orientation pointed towards the boreholes so that geophone responses could be properly compared between instruments. During insertion, X and Y tilt measurements and displacement using a string potentiometer were continuously recorded so

the final spatial coordinate and depth of each sensor was known. Rotation of the SonicWands during insertion was not measured. Figures 11a and 11b show the plan and elevation view of the sensor layout, respectively. In plan view, the sensors were arranged in a line with alternating spacing of 0.3, 0.3 and 0.4 m so that the distance between the surface projections of the outermost SonicWands was approximately 2.6 m. The nine SonicWands were pushed to three different depths (6.4, 10.4, and 14.4 m) such that there was a line of three SonicWands spaced 1 meter laterally apart at each depth. The spacing of the SonicWands was selected such that (1) the embedded geophones would show some wave amplitude decay as a result from sonic-induced wave propagation through each SonicWand, and (2) they would be as close as possible without creating difficulty for the CPT rig during insertion. Once inserted, the SonicWands remained at their depths for the duration of testing and were removed when testing was complete. Figure 12 shows a picture of the field set up after SonicWand installation had been completed.

Four sonic borings were drilled using a track-mounted drill rig at select linear offsets from the SonicWand line. The borings were drilled by an experienced driller using techniques considered to be best practice. Borings SB1 and SB2 were drilled 1.0 and 0.3 m to plan right of the surface projection of SonicWand S09, and Borings SB3 and SB4 were drilled 1.0 and 2.0 m to plan left of Sensor S1. During drilling, a string potentiometer mounted on the drill rig measured the depth of the drill bit, although the verticality of the sonic drill string was not measured. All four borings were drilled using 1.5-meter drill runs and 3-meter casing lengths, with the exception of Boring SB4, which used 3-meter drill runs. Continuous core samples were extracted from the subsurface to mimic normal drilling operations and then discarded. Borings SB1, SB2, and SB3 terminated at a final depth of 15.5 m and Boring SB4 terminated at a final depth of 17.0 m.

Geophone velocity from eight of the nine SonicWands were continuously monitored during sonic drilling, casing installation and in between sonic drill runs. Sampling frequency during drilling was 2048 Hz for Boring SB1 and 1024 Hz for the other three borings. In Borings SB1, SB2 and SB3, at a depth of 7.9 m and 10.9 m, the core barrel was removed from the borehole while the casing remained in place in order to push the post-sonic CPTs. The post-sonic CPTs were pushed from the bottom of each borehole at both depths, extending to depths of 9.25 m and 12.7 m, respectively. At the completion depth of each post-sonic CPT, the CPT rods were removed and sonic drilling resumed. The depth of the post-sonic CPTs were selected to be below the depth of the 6.3 and 10.4 meter SonicWands in order to evaluate post-sonic CPT data with SonicWand measurements from sequential drilling runs. No CPT was pushed beneath the sonic run at the 14.4-meter SonicWands because the baseline CPTs did not extend beyond that depth.

Marietta, Ohio

Phase II of the field testing program was conducted in Terra Sonic International's Yard in Marietta, Ohio and included the advancement of seven CPTs to establish baseline subsurface conditions at the site, eight SonicWands to measure soil motions during sonic drilling, and three sonic boreholes with post-sonic CPTs pushed through the borehole bottom to compare to baseline values. Baseline CPTs were pushed from February 11 to 12, 2021, and the remainder of field testing was completed from June 2 to June 5, 2021.

Site and Subsurface Conditions

Subsurface conditions at Marietta were evaluated based on a desktop review of geologic conditions and measured parameters from the seven baseline CPTs, which were advanced to a depth of about 30 m. The site is located on a floodplain approximately one-half mile northeast of

the Ohio River, and is comprised of quaternary alluvial deposits. Subsurface conditions consist of about 13 m of loose to medium dense silty sand, sandy silt and poorly graded sand, followed by a 3-meter-thick layer of dense poorly graded sand, followed by interbedded layers of loose to dense layers of silty sand, sandy silt and poorly graded sand. The groundwater table is at a depth of about 21 m below the ground surface. The CPT results for one of the baseline CPTs (CPT5) is shown in Figure 13a and a compilation of results from all seven CPTs is shown in Figure 13b. Figure 13 shows clearly that within the depths of testing (6 to 20 m), the Marietta site was on average much stiffer (average q_t of 9 Mpa) than the Salt Lake City site (average q_t of 4 Mpa).

Testing

Unlike Phase I, the SonicWands used during Phase II testing were advanced to three different depths over the course of the field tests. The general flow of the work in Phase II is summarized here:

1. Advance eight SonicWands to some nominal depth with a truck-mounted CPT rig, then drive the CPT truck off of the SonicWand array.
2. Drill three 3-meter-long sonic runs at lateral offsets of 2, 1 and 0.5 m away from the SonicWand array to a depth just past the array, then remove the drill string with the sonic casing left in place.
3. Push a CPT from the bottom of each sonic boring for 2 m.

Steps 2 and 3 of this process were then repeated, and then steps 1 to 3 were repeated. This combination of events was then repeated at two additional SonicWand depths. Figure 14 shows a flow chart of the entire field operations sequence.

During advancement, all eight SonicWands were oriented in the same direction, such that the X accelerometer orientation pointed towards the boreholes so that accelerometer responses could be properly compared between instruments. X and Y tilt measurements and displacement using a string potentiometer were continuously recorded so the final spatial coordinate and depth of each SonicWand was known, although rotation of the SonicWands was not measured. At each nominal depth, the SonicWands were arranged in a trapezoidal prism in order to achieve a geometry as close to a small cube as possible. The geometry of the SonicWand array was limited by (1) how close the CPT rig could line up over adjacent SonicWands, which was determined to be a minimum of 30 cm, and (2) the ability of the truck to drive away from the protruding cone rods attached to the inserted SonicWands. The maximum clearance of the rig was about 23 cm, so the minimum depth difference between the bottom and top planes of inserted SonicWands was about 80 cm. Thus, at each nominal depth, the SonicWand array consisted of a trapezoidal prism with a top and bottom base of 30 by 30 cm and 30 by 90 cm, respectively, and a height of 80 cm. A plan and an elevation view of the SonicWand array at each depth is shown in Figures 15a and 15b, respectively. The nominal depths of the SonicWands were 6, 12 and 18 m, which refer to the average depth of the top and bottom SonicWands in the array. The cone rod stickup of the SonicWands is shown in Figure 16.

Three sonic borings were drilled using a track-mounted drill rig at select linear offsets from the SonicWand array, as shown in Figure 17. The borings were drilled by an experienced driller using techniques considered to be best practice. Borings SB1, SB2 and SB3 were drilled 2.0, 1.0 and 0.5 m to plan right of the surface projection of SonicWands S03 and S06. During drilling, a string potentiometer mounted on the drill rig measured the depth of the drill bit, and a light sensor measured the rotational speed of the drill string. X, Y and Z accelerations were continuously

monitored during sonic drilling and during some casing installations. Sampling frequency during drilling was 2048 Hz. The verticality of the sonic drill string was not measured. All three borings were drilled using 3-meter drill runs and 3-meter casing lengths. The core barrel was advanced dry and the casing was advanced using fluid circulation. Continuous core samples were extracted from the subsurface to mimic normal drilling operations and then discarded. All borings terminated at a final depth of 20 m.

In each boring, at depths of 7.7, 10.7, 13.7, 16.8, and 19.8 m, the core barrel was removed from the borehole while the casing remained in place in order to push the post-sonic CPTs, as shown in Figure 18. The post-sonic CPTs were pushed from the bottom of each borehole at all five depths extending for a depth of 2 m. At the completion depth of each post-sonic CPT, the CPT rods were removed and sonic drilling resumed. At a depth of 16.9 m, boring B2 had to be flushed with water in order to advance the CPT through the soil that had heaved into the casing. At a depth of 19.8 m, the CPTs in Borings B1 and B2 could not be pushed through soils that had heaved into the casing.

RESULTS AND ANALYSIS

Sonic Drilling Performance

The performance of the sonic rig, including the vibrational content of the drill string and soil are discussed in this section. Data recorded during the sonic drilling are presented here, including displacement, velocity and acceleration time histories of the drill string, the rotational speed of the drill string, the frequency content of the drill string, and the time histories recorded by the geophones and the accelerometers in the SonicWands.

Herein the data recorded from four primary drill runs, two from Phase I and two from Phase II, are presented and discussed. From Phase I, the drill runs are Boring SB1 from 6.4 to 7.9 m and Boring SB2 from 9.4 to 10.9 m, and will be referred to as Runs 1A and 1B. From Phase II, the drill runs are Boring SB3 from 4.6 to 7.6 m and Boring SB3 from 10.7 to 13.7 m, and will be referred to as Runs 2A and 2B. The data recorded from Phase I varied in terms of the duration of drill run and induced soil motions, but the trends that emerge from the data are best demonstrated by Runs 1A and 1B. Data from Phase II tends to be much more consistent and is demonstrated well by Runs 2A and 2B. For brevity's sake, the four drill runs described above are the primary data discussed in this Thesis. Table 1 summarizes the drill run information and the depth of the SonicWands that were passed by (or were closest to) the bit during the drill run. The remainder of the time histories from Phase I are presented in Appendix A.

Sonic Drill Motions

String potentiometer measurements during sonic drilling were used to determine the displacement, velocity, and acceleration time histories of each sonic run. The string potentiometer displacements were affected by the vibrations of the drill rig, so the raw measured drill string

displacements were smoothed using an n-point running average (where n varies from 1000 to 2000, depending on the sampling frequency) to effectively filter out vibrational contributions. The smoothed drill string displacements were then differentiated using the time interval between sampling points (e.g. $dt = \frac{1}{f_s} = 0.000977$ for $f_s = 2048$) to determine the drill string velocity. The velocity was again smoothed using an n-point running average (which varied from 200 to 1000 points) and differentiated to determine the acceleration. The displacement, velocity, and acceleration of the drill string during Runs 1A and 1B are shown in Figures 19a and 19b, and Runs 2A and 2B are shown in Figures 20a and 20b. Runs 2A and 2B also include the average rotational speed in (rotations per second) of the drill string measured by the light sensor. Figures 19a and 19b clearly show that the duration of two drill runs of equal length can take very different times to complete, in this case, 60 and 25 seconds. The drill run for Phase I Boring SB3 from 6.4 to 8.0 m (same depth range and soil type as Figure 19a) is shown in Figure A9 in Appendix A and took 6 seconds. A longer drill run will subject the surrounding soil to more vibrations, while a shorter one will be subjected to a greater down pressure.

Soil Motions

Vibrations propagating through the soil due to sonic drilling were continuously monitored in the X (radial), Y (circumferential) and Z (vertical) directions (relative to boring) by the SonicWand geophones in Phase I and accelerometers in Phase II. Figure 21a shows the recorded X geophone velocities during Run 1A, corresponding to the same drill run as Figure 19a. Figures 21b, 22a, and 22b show Runs 1B, 2A, and 2B, respectively, and correspond the same drill runs as Figures 19b, 20a, and 20b. The three colors of the plots show X-direction (longitudinally propagating waves) time histories recorded in the SonicWands located at their respective lateral distances away from the sonic boring. For Phase I, these distances range from 0.3 to 3.3 m, and in

Phase II, these distances are 0.5 to 1.1 m (time histories from the 1.4 meter SonicWand and the second row of SonicWands are not shown in this plot to more clearly show the 0.5, 0.8 and 1.1 meter time histories). The black line shows the depth of the drill tip as it moves through the subsurface. Consequently, in Figure 21b, the drill tip passes the depth of the SonicWands (10.4 m) at about 14 seconds into the drill run. In Figure 21a, sonic drilling commenced roughly at the depth of the closest SonicWands. Note that in Phase I, the SonicWands shown in these plots were in a linear array and all at the same depth; in Phase II, the SonicWands were in a trapezoidal array and therefore at two separate depths. Thus, in Figures 22a and 22b the drill string passes the plane of the upper SonicWands (0.8 and 1.1 meter offsets) before the lower SonicWands (0.5 and 1.4 meter offsets, although the 1.4 meter offset SonicWand time history is not shown here). As expected, there is a time delay in the peak amplitude recorded by the accelerometers, which can be seen clearly in Figure 22a. The SonicWand at 0.5 m offset (in the lower plane) shows a peak in acceleration about 1.5 seconds after the SonicWands at 0.8 and 1.1 m offsets (upper plane) do. At this moment, the drill string velocity is about 0.5 m per second (Figure 20a). Therefore, the drill bit has travelled an estimated distance of about 0.75 m, close to the actual vertical distance of 0.8 m between the upper and lower SonicWands. Figures 22a and 20b also show the velocity time history recorded by the accelerometers in Phase II. The velocities were found by numerically integrating the recorded acceleration time history. The acceleration time history was filtered using a high pass filter with a corner of 50 Hz and any signal drift was removed by subtracting out a least-fit squares linear drift.

Figures 21 and 22 ostensibly show that the maximum velocity amplitude of the soil motions recorded in Marietta is approximately 10 times greater than the maximum velocity amplitude recorded in Salt Lake City at similar distances away from the drill string (e.g. 0.01 m/s in Marietta

compared to 0.001 m/s in Salt Lake City). However, it should be noted that in many cases the geophone velocity saturated due to the magnitude of the drill string motions, so it is difficult to determine what the maximum velocity truly was at the Salt Lake City site. Additionally, as mentioned previously, the accelerometers used to measure the soil motions in Phase II had a range of 200g, which proved to be much too large for the magnitude of vibrations induced by sonic drilling. Consequently, the signal-to-noise ratio for the Phase II recordings is large, and the peak amplitude shown in the figures is likely affected by the noise level. Regardless, it is expected that the magnitudes of the amplitudes shown in the time histories are within an order of magnitude of being correct. It is also evident from Figures 21 and 22 that soil motions tend to be greater closer to the drill string; however, many factors contribute to the soil response, as discussed in more detail below. Some of those factors may include soil type (e.g. stiffness), rig velocity/down force, rig frequency content, vibrational amplitude, drilling speed and drilling duration.

In Figures 21 and 22, the frequency content in the three time histories for each plot is shown in terms of Fourier amplitudes. The frequency contents tend to be very similar for all three SonicWands (i.e. the dominant and harmonic frequencies do not vary with distance), with an amplitude decrease with increasing distance away from the drill string. This frequency content represents the overall frequency content measured in the SonicWands over the duration of the sonic run, and is expected to match the frequency content of the drill rig. The dominant frequency is taken to be the frequency with the highest amplitude, which corresponds to the driller "locking in" to the system resonance frequency. Recall that the system resonance frequency is the frequency at which the entire system of drill string and soil are in a resonance condition (Massarsch et al. 2021).

The system resonance frequency from each drill run for all seven borings from both phases was plotted against the average depth of the drill run (e.g. a drill run from 6.4 to 7.9 m would have an average depth of 7.2 m), shown in Figure 23. As expected, and consistent with Equation 1, the system resonance frequency decreases with increasing depth and is confined to the operational range of the drill rig, about 50 to 170 Hz. Essentially, the driller is trying to achieve resonance (or close to resonance) for a given depth using the available frequency range of the rig. In Phase I (shown in black and gray) from about 0 to 5 meters, the driller is operating at what could potentially be the first undertone of the system resonance frequency in order to achieve resonance during the run. Around 4 to 8 meters, fundamental resonance frequencies becomes available to the driller, so the driller switches up to those frequencies as shown by lower black line in Figure 23. If the operational range of the drill rig was extended to higher frequencies (i.e. above 170 Hz), one might expect that the system resonance frequency at shallow depths would follow the grey dashed curve rather than the upper solid black line. The grey dashed line follows the grey points, which are 2 times the measured values at a given depth (e.g. the first undertone multiplied by 2 is the fundamental tone). The result is a single curve, shown by the continuous lower solid black line and the grey line, which would be the expected frequencies at a given depth for a rig with a wide operational range. The Phase II curve, shown in red, shows a very similar curve to that of Phase I. The light red diamonds represent two times the measured data, and the dashed trendline extending beyond 170 Hz represents the expected depth/frequency relationship if the drill rig was capable of vibrating at those frequencies. The Phase II data is very similar in shape to Phase I, but is shifted to the right (i.e. the frequency at a given depth for Phase II is slightly higher than for Phase I). This suggests that the system resonance is affected by the overall composition of the soil, and that a stiffer soil profile (in theory, an increase in the variable c in Equation [1]) would increase f_n for a

given length of drill string. This is shown by the curve for the stiffer Marietta site, which is shifted to the right relative to the less stiff Salt Lake City site. As expected, the actual curves are significantly less than a curve predicted by equation [1] using c equal to 5,030 m/s (i.e. the resonance frequency for a steel rod not in contact with soil.). This is due to wave reflection and interference from joints in the drill string, energy attenuation from soil friction along the shaft, and contact with the soil at the sonic tip.

Dynamic Frequency Content

Figures 21 and 22 show the frequency content of the sonic drill run, but it is useful to plot how the frequency content changes with time (dynamic frequency), and compare the dynamic frequency content to soil parameters, as well as drill string and soil motions. Figures 24a and 24b show the dynamic power spectral density of the Phase I drill runs as they penetrate downward, alongside the velocity of the drill runs and the q_t profile of the closest baseline CPT sounding (in this case CPT7). Figures 25a and 25b show the same for the Phase II drill runs. Because the frequency and velocity are initially measured against time, plotting these variables against depth results in an asymptotic trend near the plot bounds where the drill begins to slow to zero velocity. The spectrograms show a dynamic frequency history for the X direction in a single SonicWand. The lateral distance between the SonicWand and the boring is 1.3, 0.3, 0.5 and 0.5 m for Figures 24a, 24b, 25a, and 25b, respectively (i.e. they show the dynamic frequency content of the closest time history shown in each plot of Figures 21 and 22).

In Figure 24a, there are clear frequency and amplitude increases at depths of 7.2 and 7.7 m, corresponding to the large increases in geophone response at the same depths (Figure 21a). Furthermore, the frequency increase at 7.7 m aligns with a stiff sandy layer being encountered and

a reduction in penetration velocity. The two significant high-amplitude first-mode frequencies of approximately 80 and 100 Hz can be seen in Fourier amplitude plot of Figure 21a, and higher frequency modes have accordingly lower magnitudes. Although Figure 24b shows a relatively constant dynamic frequency with minor fluctuations in q_t, the q_t spike at 10.8 m corresponds to a decrease in penetration rate, increase in vibrational frequency, and increase in the geophone response, similar to Figure 24a. At about 10.9 m, the drill string vibration pauses and the velocity and frequency go to zero, which is seen by the lack of geophone response in Figure 21b at about 20 seconds. These trends are not as apparent in Figures 25, where the q_t profile and dynamic frequency during the drill runs are relatively constant. Interestingly, in Figure 25b, the driller begins vibrating at the system resonance frequency fairly late into the drill run, after about 1 meter of penetration has already occurred. These figures show that the frequency content of a drill run does not seem to have an effect on the soil response.

Comparison of CPT Values

As a means of quantifying the amount of disturbance induced by sonic drilling, baseline CPT data was plotted against and compared to post-sonic CPT data. Here, changes in the measured tip resistance (either q_t or Q_{tn}) between baseline and post-sonic CPTs that cannot be accounted for by spatial variability are attributed to being due to sonic disturbance. Figures 26 through 36 show tip resistance data from post-sonic CPTs pushed beneath sonic borings along with the baseline CPTs surrounding the sonic borings. The depths of the post-sonic data begin immediately below the base of the sonic borehole (for example, Figure 26 shows CPT data from 7.9 to 9.2 m, immediately beneath the drill run shown in Figures 19a and 21a). The upper left plot shows measured q_t or Q_{tn} profiles for the baseline and post-sonic CPTs, which is divided into four depth

intervals. The depth intervals were selected at boundaries of what was considered disturbed/not disturbed as well as boundaries of tip resistance behavior, or in other words, similar parameter characteristics. The baseline and post-sonic parameter profiles were sorted by q_t (or Q_{tn}) for each depth interval to compute the cumulative distribution, shown in the four bottom plots. The median, 16th, and 84th percentile values for each of the four cumulative distributions are shown in the upper right plot of the figure, which illustrate a direct comparison of the overall q_t (or Q_{tn}) response at different depths for the baseline and post-sonic values. For two of the CPT runs, Q_{tn} values were analyzed in addition to q_t values to rule out the effects of overburden stress on the measured tip resistances.

Table 2 summarizes the information contained within each figure, including the parameter to be compared (either q_t or Q_{tn}); the baseline and post-sonic CPTs that were analyzed; the depth range of the CPT; the median q_t, median I_c, and material type found in the upper depth interval (based on SBT); the depth of disturbance; and percent difference in measured median value of baseline and post-sonic tip resistance in the upper depth interval. The depth of disturbance has been quantified here as the depth from the start of the post-sonic CPTs to where changes in the 16th, median and 84th percentiles of tip resistance are more likely due to spatial variability than sonic drilling influence. The percent difference is calculated by equation [2]:

$$\%\ Difference = \left|\frac{Baseline\ median - Post\ sonic\ median}{Baseline\ median}\right| \times 100\% \qquad [2]$$

For example, the first depth interval in Figure 26 shows that the median values for the baseline and post-sonic CPTs are 0.76 and 0.18, respectively, which differ by a 76 percent. A value greater than 100 percent indicates that the post-sonic CPTs resulted in a larger tip resistance than

the baselines. Tip resistance increase is likely due to heaving of sand into the casing when the core barrel was removed after drilling.

Figures 26 through 36 show that within a range of 0.2 to 0.7 m beneath the base of a sonic borehole, measured tip resistance values are almost always reduced after sonic drilling has occurred. The data presented here indicate that this reduction can be as much as 90 percent for q_t, and this reduction is higher in clay-like materials (36 to 90 percent reduction, Figures 26 to 30) than those that are closer to sand (24 to 67 percent reduction, Figures 31 to 36). The post-sonic CPT profiles in clay-like materials are characteristically lower than the baseline values to some depth beneath the casing, generally 0.2 to 0.4 m. Pore pressure data obtained from Phase I suggests that the excess pore pressure generated by sonic drilling is very small; therefore, this decrease in tip resistance is likely not due to excess pore pressures. In some cases in sandy materials, the post-sonic tip resistance begins below the values recorded by the baseline CPTs, then increases very rapidly above the baseline values, only to equilibrate with them shortly thereafter (Figures 33 and 35). This phenomenon can potentially be explained by material that is within the boundary confined by the sonic casing. At the surface of the material, there is no confining pressure, thus tip resistance values are low. As the CPT advances, the material cannot displace around the tip because of the casing, resulting in much higher tip resistances. The CPT then moves below the bottom of the casing and the tip resistances reflect the baseline values. It should be noted that soil that is within the casing is considered slough and the post-sonic CPT values are not regarded as being meaningful in evaluating sonic-induced disturbance. CPT profiles where the tip resistance doesn't rapidly increase above the baseline values likely begin at or below the depth of the casing and are therefore not affected by it (Figures 31 and 34). Figure 34 shows lower q_t values past the characteristic low section, suggesting that this section is affected by vibrations while others are

not. Beneath a depth of 0.2 to 0.7 m below the bottom of the casing, there appears to be no effect whatsoever on tip resistance values, and differences between baseline and post-sonic values can be attributed to spatial variability. Beneath this depth, it appears that the soil motions are primarily elastic strains that do not produce permanent plastic soil deformations.

The duration and intensity of vibration may be positively correlated to soil disturbance. For example, consider the sonic run in Phase I at a depth of 6.4 to 7.9 m (primarily clay with two sand lenses), as seen in Figure 21a, which shows the X geophone velocity for Boring SB1 and displays some saturation at 1.3 and 2.3 meter offsets. Table 2 indicates that immediately following this drill run, the baseline to post sonic tip resistance changed by 76 percent. Data for Phase I Boring SB3 at the same depth as Figure 21a is shown in Figure A9 in Appendix A, and the time histories display much less saturation for a shorter duration than Figure 21a at equivalent offsets. The change from baseline to post-sonic tip resistance is 36 percent, which is far less than 76 percent, indicating that the duration and intensity of vibration may influence the amount of disturbance the soil experiences. Unfortunately, the time histories recorded in Phase II are not high quality enough to provide additional evidence for this claim. However, The CPT comparisons in Phase II show that soils at increasing depths appear to have similar changes in post-sonic CPTs to those at shallower depths. Because the vibrational frequency of the sonic drill is directly related to depth, it would follow that frequency content is not a factor in these data. It therefore appears that a primary factor in the magnitude of disturbance is soil type and potentially vibrational intensity and duration. Other factors that have not yet been explored are mechanistic components of the sonic drill rig (down pressure) and other typical rig operations (e.g. borehole flushing).

The evidence presented here contradicts the claims made by Wentz and Dickenson (2013) and Watkins et al (2020), which purport that SPTs performed below the base of a sonic boring were not significantly different from those performed beneath the base of a mud rotary boring (i.e. not affected by vibrations). The data in this Thesis suggests that there is some amount of disturbance due to sonic drilling, although the amount of disturbance is minimal.

CONCLUSIONS

This study attempted to investigate the effects of sonic drilling on soil disturbance by conducting two field tests. The field tests measured soil motions due to sonic drilling, as well as baseline and post-sonic CPTs, which were then compared to evaluate the effects of sonic drilling on the CPT parameters. Conclusions from the field study include:

- Penetration rates during sonic drilling runs vary. The measured penetration velocities for a sonic drill run in this study ranged from about 0.04 to 0.5 m/s, and accelerations ranged from about 0.02 to 0.7 m/s^2. The duration of a sonic drill run will likely depend on the force exerted on the drill string and will affect the amount of vibrations induced in the surrounding soil.
- To achieve system resonance during drilling, the rig operator decreased the vibrational frequency with increasing depth (i.e. with increasing drill string length), as expected. The system resonance frequency is dependent on the soil stiffness, and increases for a given depth with stiffer soil. The range of available frequencies dictate what frequency a driller can select during penetration.
- The method by which the driller operates the rig (e.g. choice of frequency, penetration velocity) may be dependent on the encountered soil type. In this study, encountering stiffer layers (as indicated by an increase in q_t plots) often resulted in decreased penetration velocity and increased sonic frequency. At this stage in the research, it is unclear what part frequency content and penetration velocity play in affecting the measured soil motions.
- Disturbance from sonic drilling was evaluated by comparing cumulative distributions of tip resistance measurements (q_t and Q_{tn}) from baseline and post-sonic soundings. Measurements up to 0.2 to 0.7 meters below the sonic casing generally showed smaller values in post-sonic

soundings, ranging from 24 to 90 percent smaller than the baseline measurements. One post-sonic sounding was 140 percent larger than the baseline measurements. This indicates that some sonic-induced disturbance had occurred, which may be due to vibrations, lack of confinement or heaving material. At depths of 0.2 to 0.7 m below the casing, spatial variability appears to dominate differences between baseline and post-sonic CPTs. The magnitude of the disturbance in these data appears to be governed more by soil type and vibrational intensity/duration than depth and frequency content and appears to be more significant for clay-like soils. Other factors that influence the amount of disturbance may be rig down pressure as well as drilling techniques, such as borehole flushing. Additional study is required to evaluate these factors further.

REFERENCES

ASTM Standard D1586/D1586M – 18. 2018. Standard Test Method for Standard Penetration Test (SPT) and Split-Barrel Sampling of Soils. ASTM International, West Conshokocken, PA.

Barrow, J.C. 1994. The Resonant Sonic Drilling Method: An Innovative Technology for Environmental Restoration programs, *Ground Water Monitoring and Remediation*, 153 – 160.

Lucon, P.A. 2013. Resonance: The Science behind the Art of Sonic Drilling (Doctoral Dissertation).

Massarsch, K.R., Wersall, C., Fellenius, B.H. 2021. Vibratory Driving of Piles and Sheet Piles – State of Practice. *Proceedings of the Institution of Civil Engineering – Geotechnical Engineering,* https://doi.org/10.1680/jgeen.20.00127.

Watkins et al. 2020. Investigation into Effect of Sonic Drilling Methodology on Standard Penetration Test Results in Dense Sand. *Geotechnical Testing Journal*.

Wentz, F.J. and Dickenson, F.E. 2013. Pore Pressure Response during High Frequency Sonic Drilling and SPT Sampling in Liquefiable Sand. *19th NZGS Geotechnical Symposium*, Dunedin, New Zealand.

Van Horn, R. 1982. Surficial Geologic Map of the Salt Lake City North Quadrangle, Davis and Salt Lake Counties, Utah. USGS. Miscellaneous Investigations Series Map I-1404.

Table 1 – Summary of drill runs performed at the Salt Lake City and Marietta Sites.

Phase	Run Name	Boring	Sonic Run Depths (m)	SonicWand Depth (m)
I	1A	SB1	6.4 to 7.9	6.4
I	1B	SB2	9.4 to 10.9	10.4
II	2A	SB3	4.6 to 7.6	6*
II	2B	SB3	10.7 to 13.7	10**

*Nominal depth of SonicWand Array. Actual SonicWand depths are 5.6 and 6.4 m.

*Nominal depth of SonicWand Array. Actual SonicWand depths are 9.6 and 10.4 m.

Table 2 – Summary of CPT soundings analyzed.

Figure	Phase	Parameter	Baseline CPTs	Post-sonic CPTs	Post-sonic depth range (m)	Median q_t (MPa)	Median I_c	Material Type	Disturbance Depth (m)	Percent Difference (%)
26	I	q_t	CPT2, CPT5, CPT7	SB1, SB2	7.9 – 9.25	0.76	2.85	Clay	0.4	90
27	I	Q_{tn}	CPT2, CPT5, CPT7	SB1, SB2	7.9 – 9.25	0.76	2.85	Clay	0.4	76
28	I	q_t	CPT1, CPT3, CPT6	SB3	7.9 – 9.2	0.75	2.9	Clay	0.2	36
29	I	q_t	CPT2, CPT5, CPT7	SB1, SB2	10.9 – 12.7	2.7	2.8	Clayey Silt to Silty Clay	0.3	84
30	I	q_t	CPT1, CPT3, CPT6	SB3	10.9 – 12.8	1.9	2.8	Clayey Silt to Silty Clay	0.3	89
31	II	q_t	SP02, CPT5, CPT7, CPT9	SB1, SB2, SB3	7.7 – 9.8	5.1	2.1	Sand to Silty Sand	0.2	11
32	II	Q_{tn}			7.7 – 9.8	5.1	2.1	Sand to Silty Sand	0.2	16
33	II	q_t			10.7 – 12.8	9.2	2.0	Sand	0.3	67
34	II	q_t			13.7 – 15.8	12.7 – 15	1.9	Sand	0.7	28 – 37
35	II	q_t			16.7 – 18.8	8.7 – 11.8	2.2	Sand	0.2	24 - 140
36	II	q_t			19.8 – 21.8	10.3	2.2	Sand	0.0	0

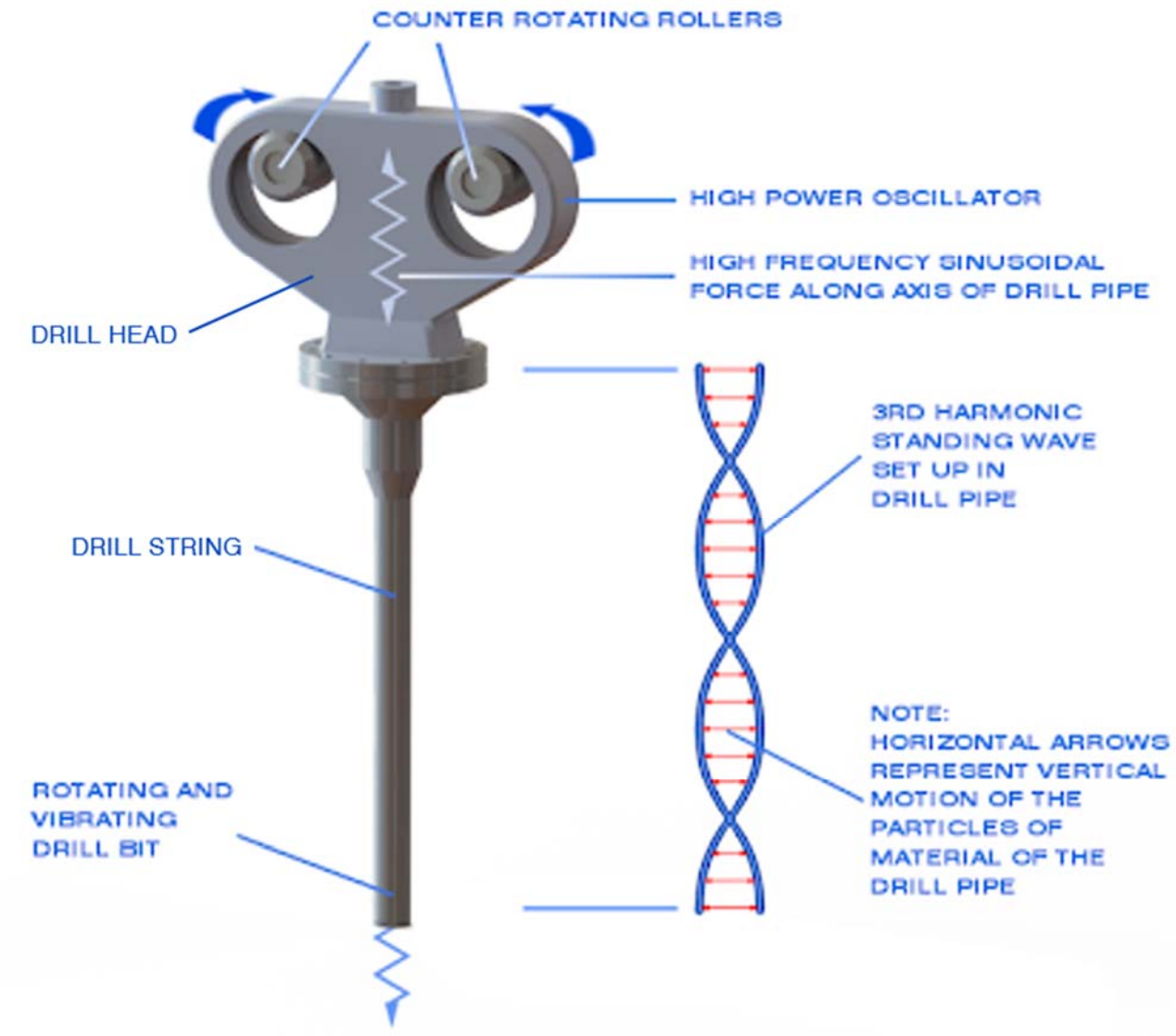

Figure 1 – Sonic drilling schematic (from Sonic Drill Corporation).

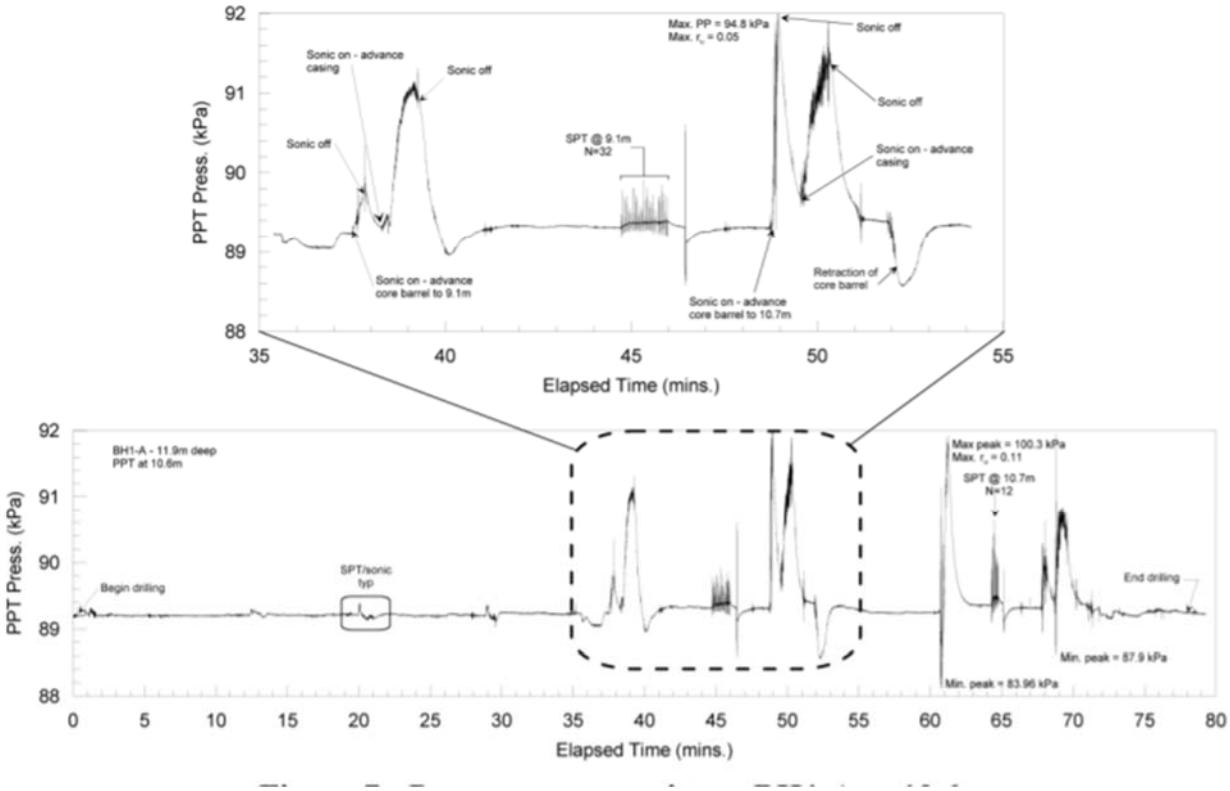

Figure 2 – Pore pressure dissipation during sonic drilling (from Wentz & Dickenson 2013).

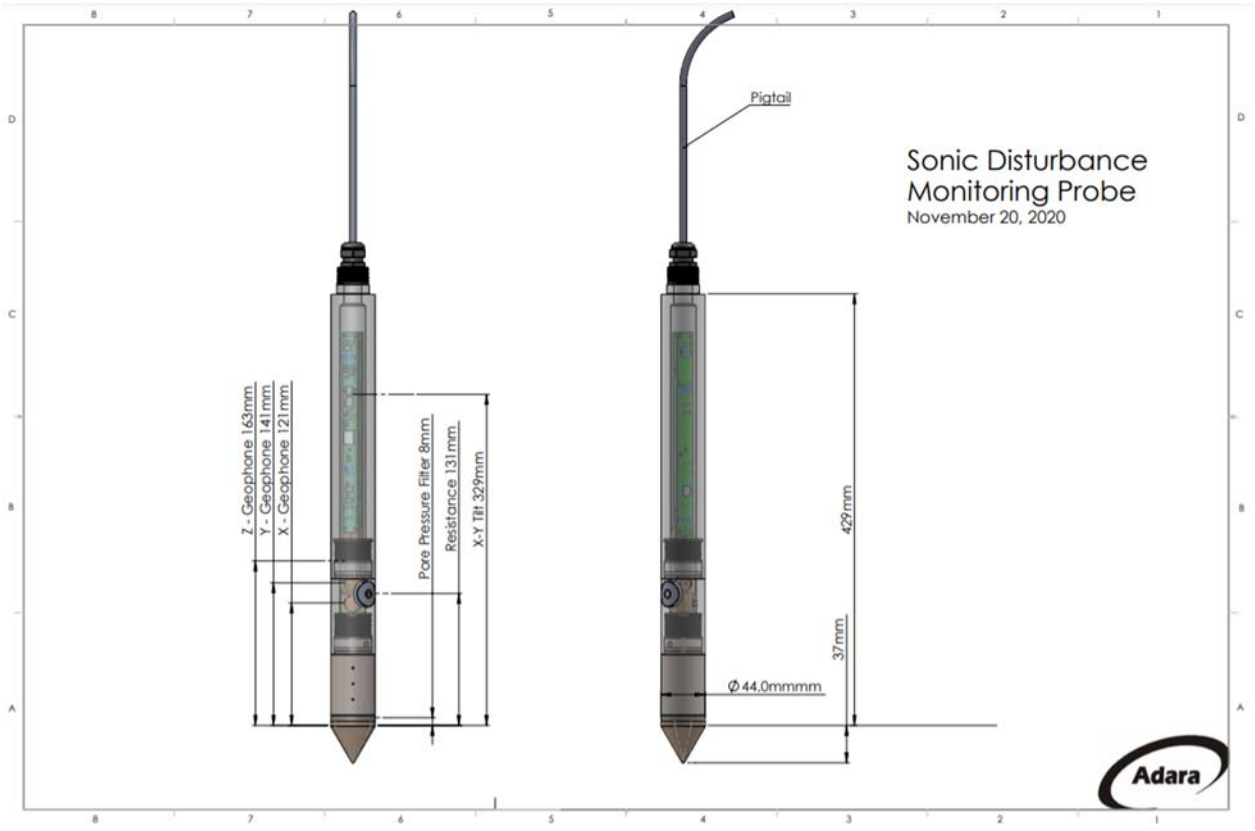

Figure 3 – SonicWand schematic. Note that the label ‘resistance’ refers to a temperature gauge.

Figure 4 – Manufactured SonicWand.

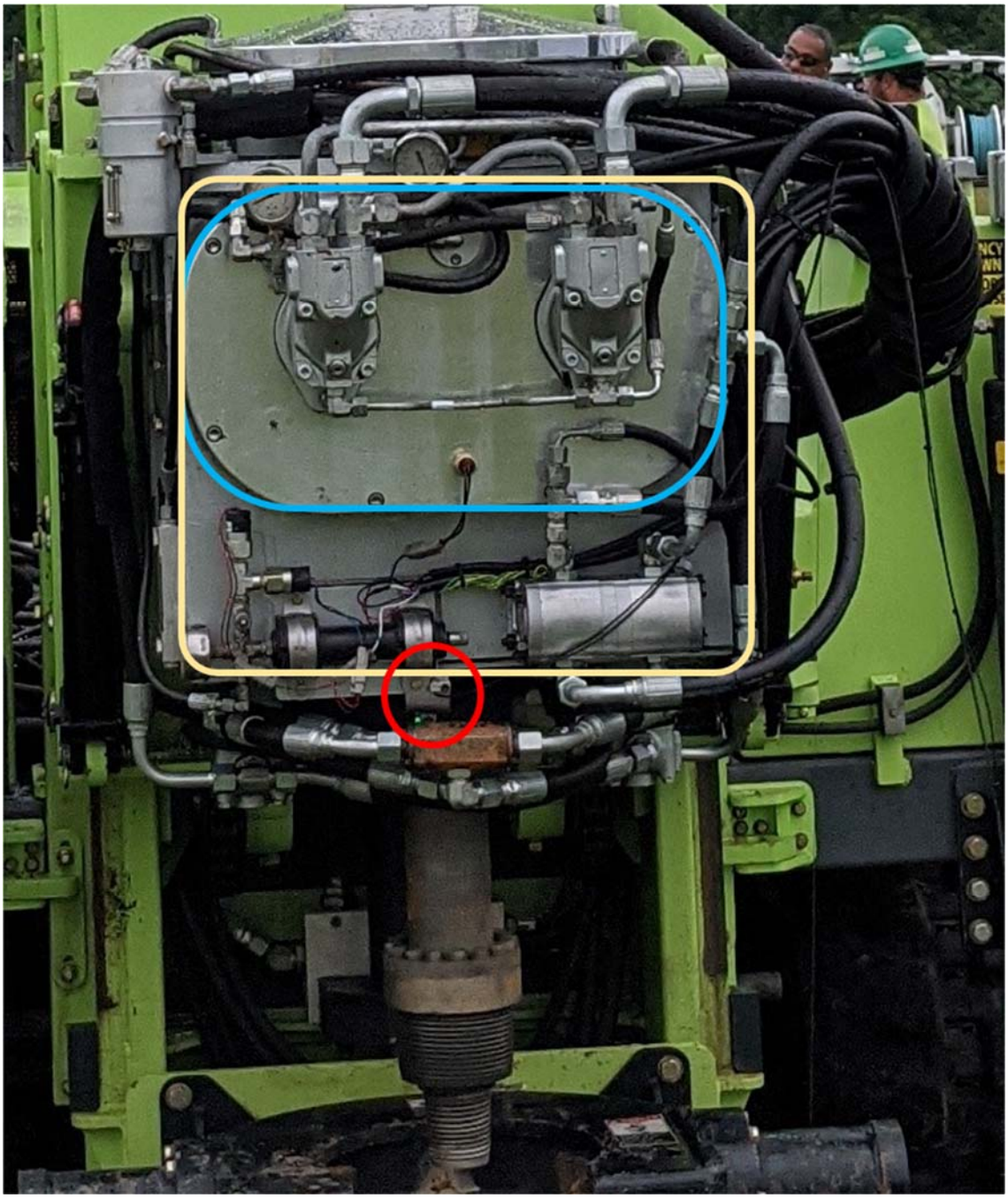

Figure 5 – Sonic head with the mounted light sensor mounted on the tub. The oscillator is outlined in blue, the air cushion in yellow. The L-bracket is circled in red, and the sensor (which has a small green light) is mounted on the L-bracket facing towards the drill shaft (into the page).

(a)

(b)

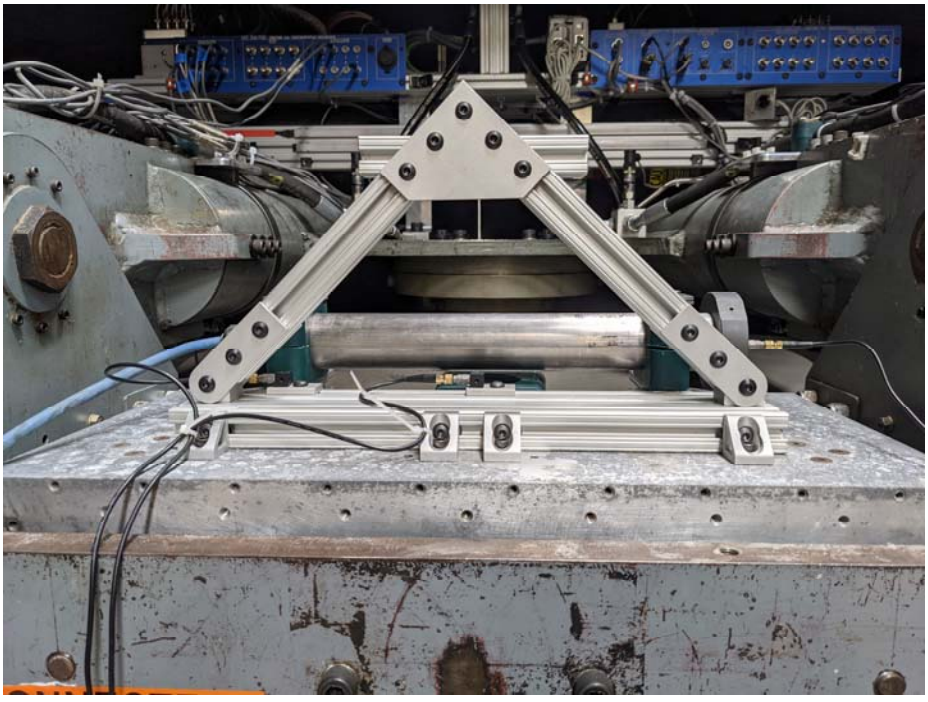

Figure 6 –Mounting for SonicWand calibration in the (a) X/Y direction and (b) Z direction.

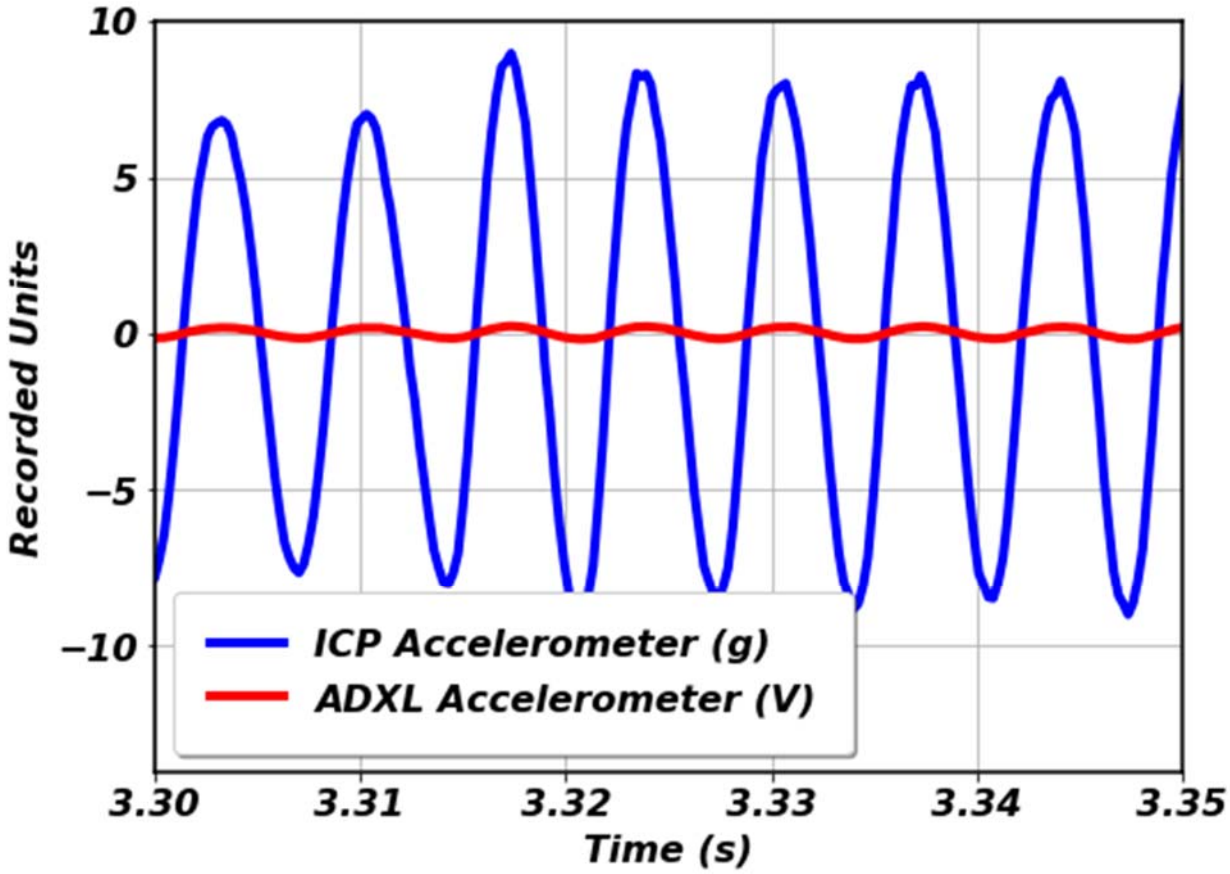

Figure 7 – Sample recorded non-normalized signals for Z geophone calibration.

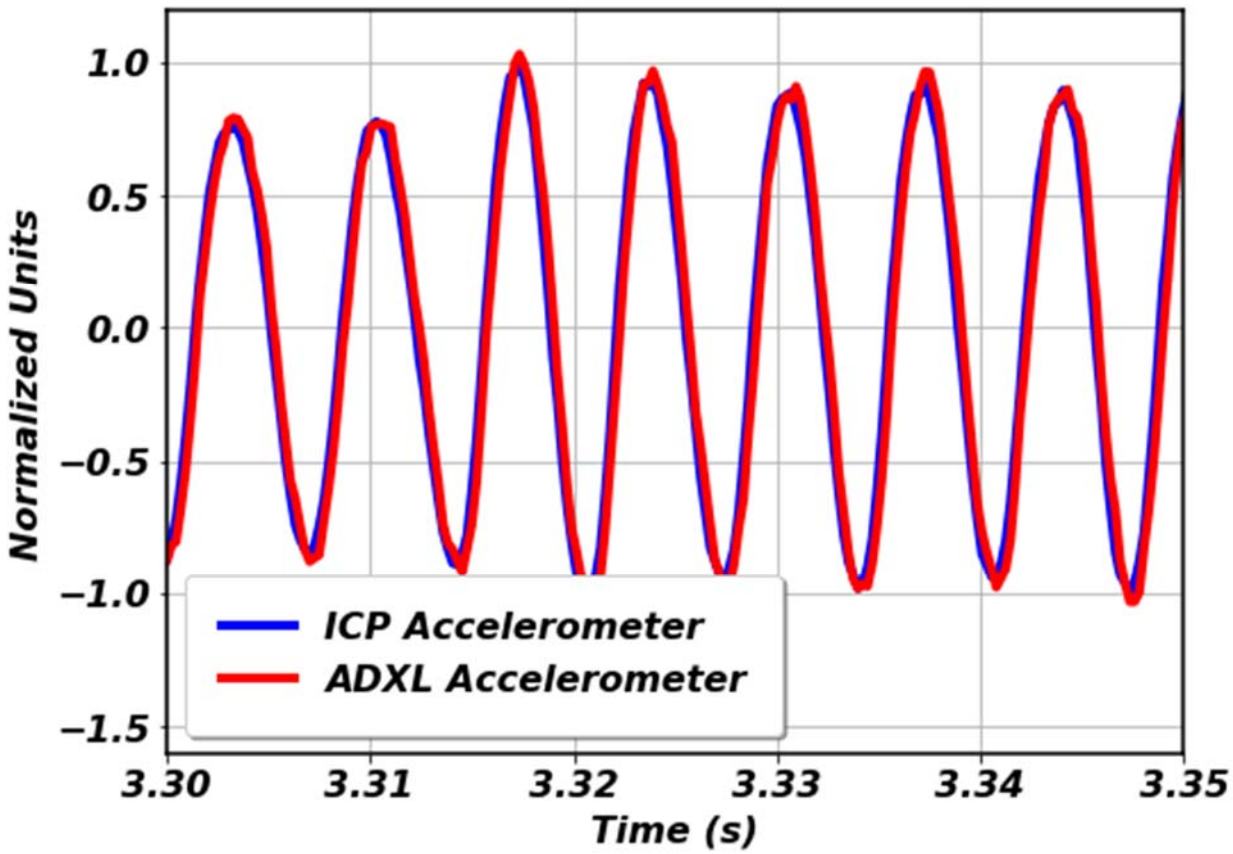

Figure 8 – Sample recorded normalized signals for Z geophone calibration.

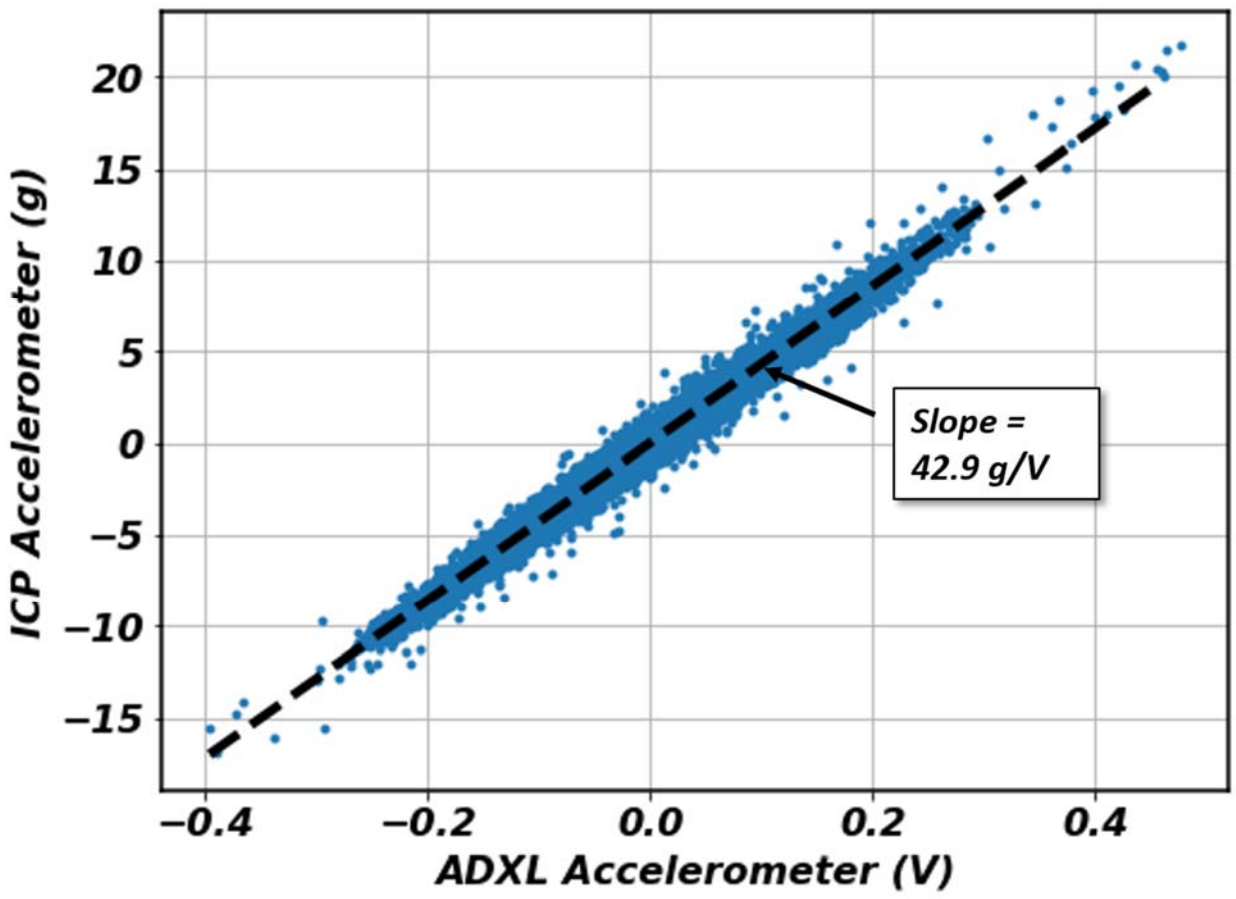

Figure 9 – Sample recorded signals for Z geophone calibration with best-fit line (calibration factor).

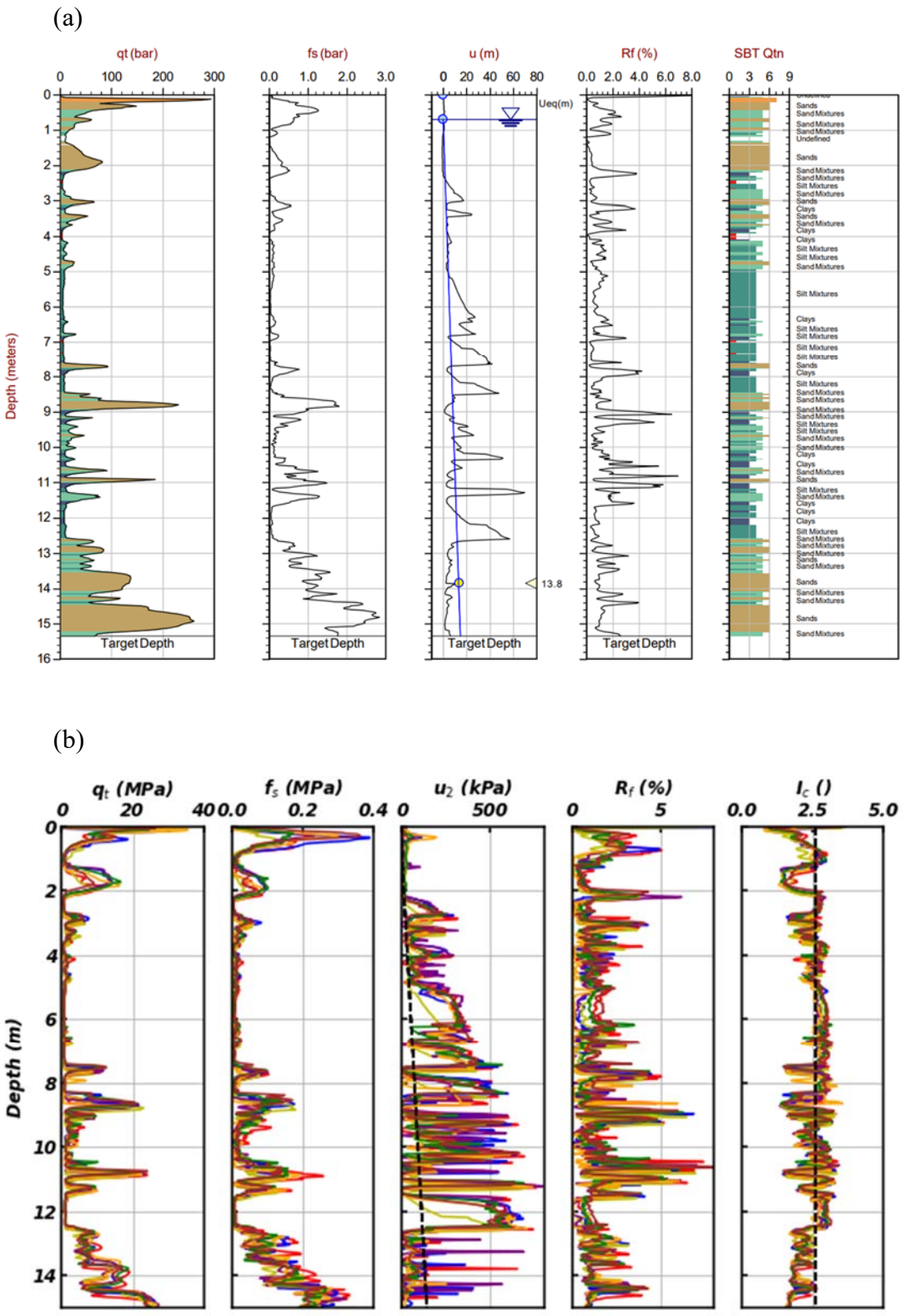

Figure 10 – Phase I CPT results, (a) CPT7 and (b) compiled for all seven CPTs.

(a)

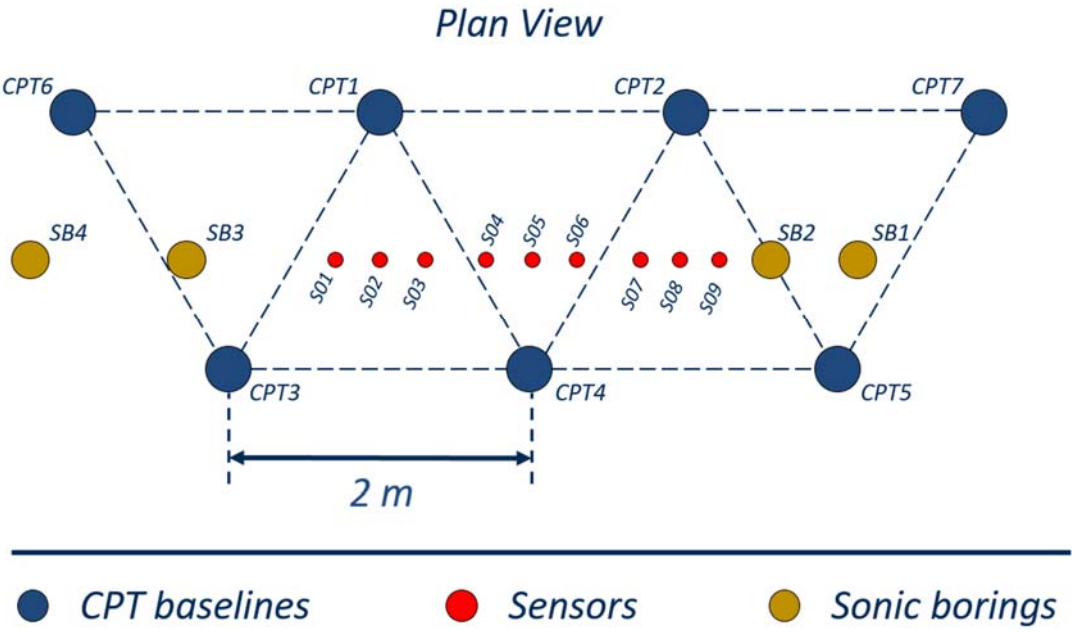

(b)

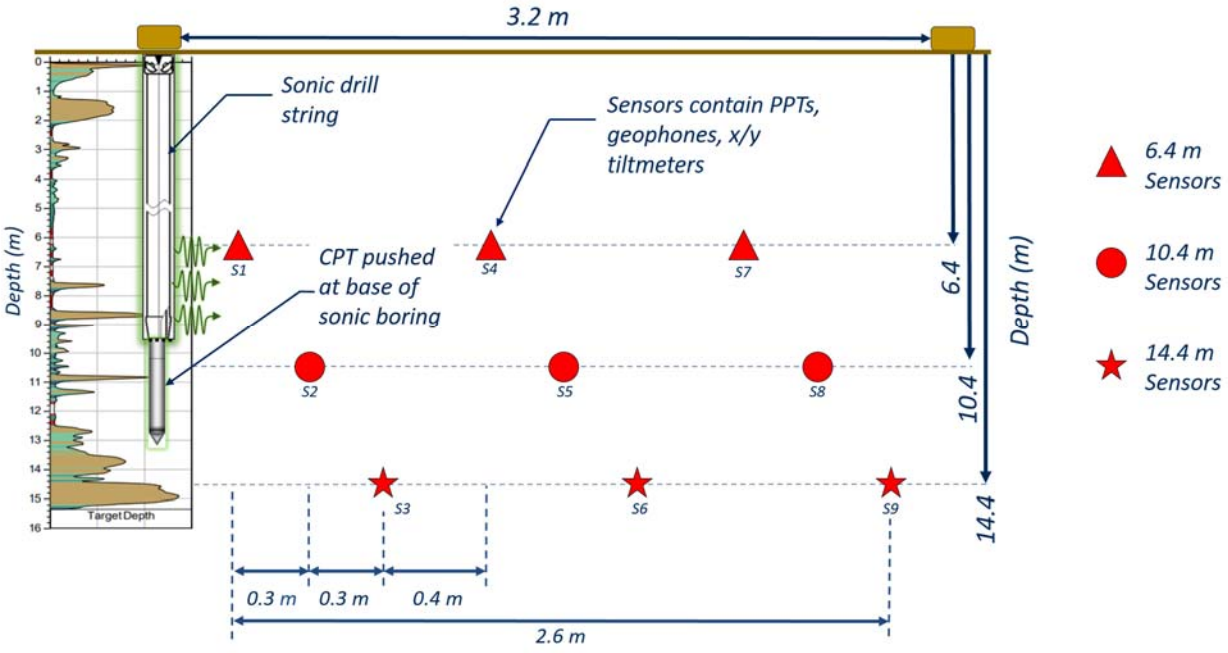

Figure 11 – Phase I testing layout, (a) plan view and (b) profile view.

Figure 12 – Phase I field setup. The cone rods attached to the SonicWands are protruding from the subsurface. The orange markings on the ground indicate where the baseline CPTs were pushed.

(a)

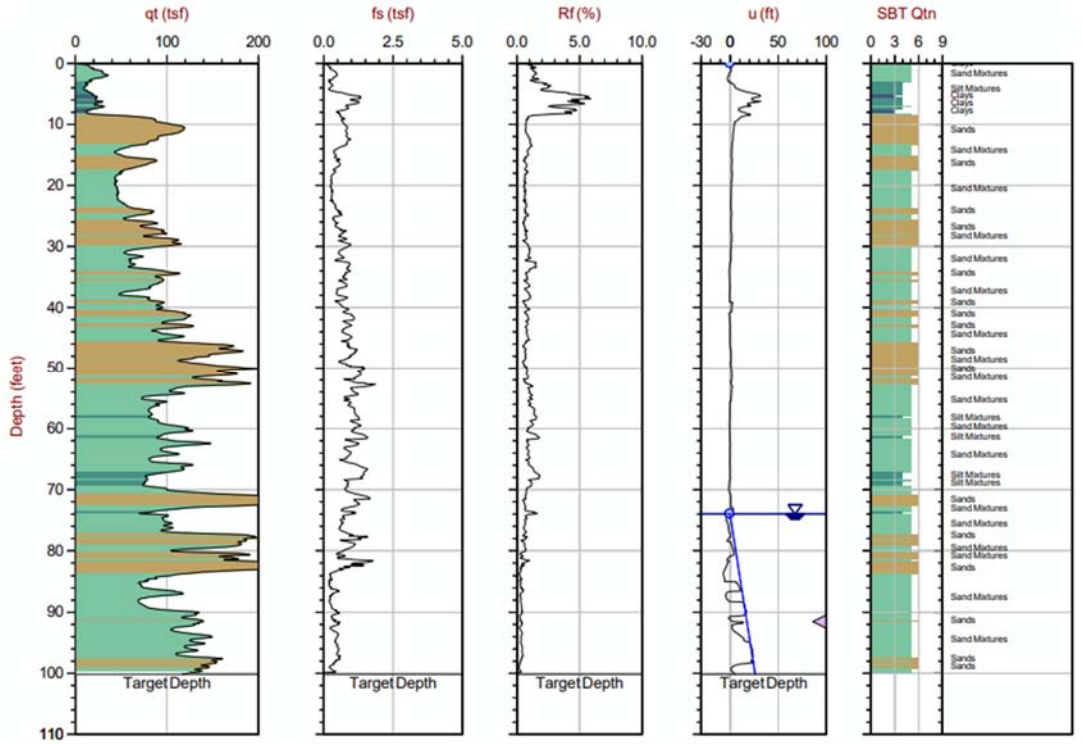

(b)

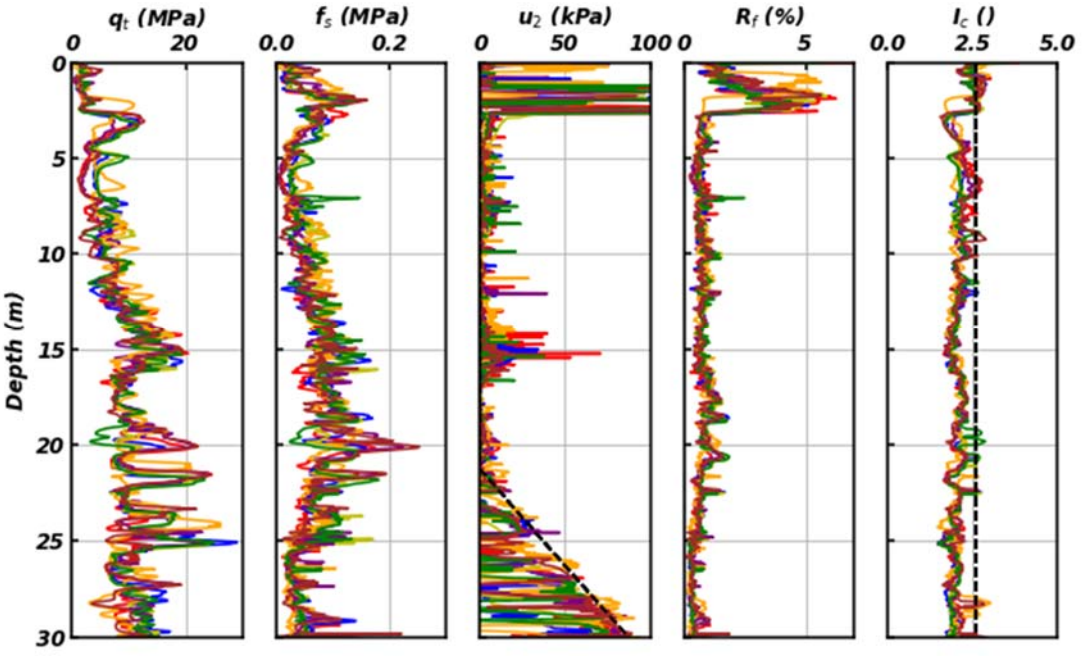

Figure 13 – Phase II results, (a) CPT 5 and (b) complied for all CPTs.

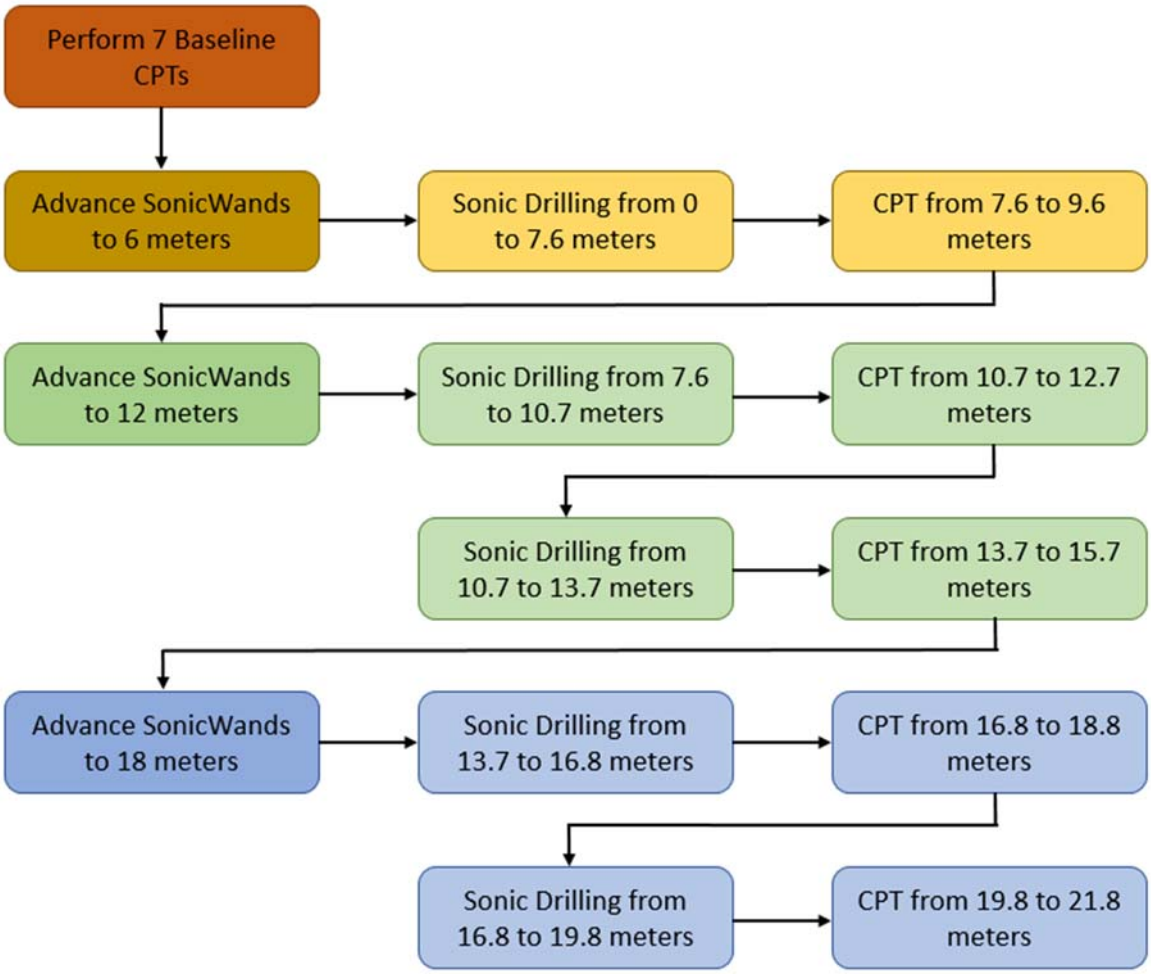

Figure 14 – Flowchart detailing Phase II field operations.

(a)

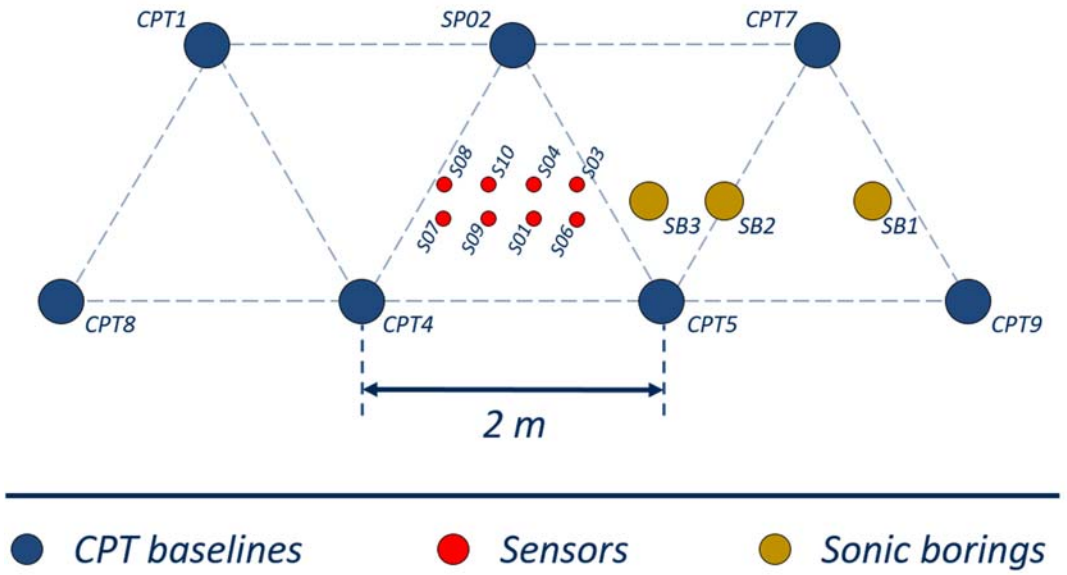

(b)

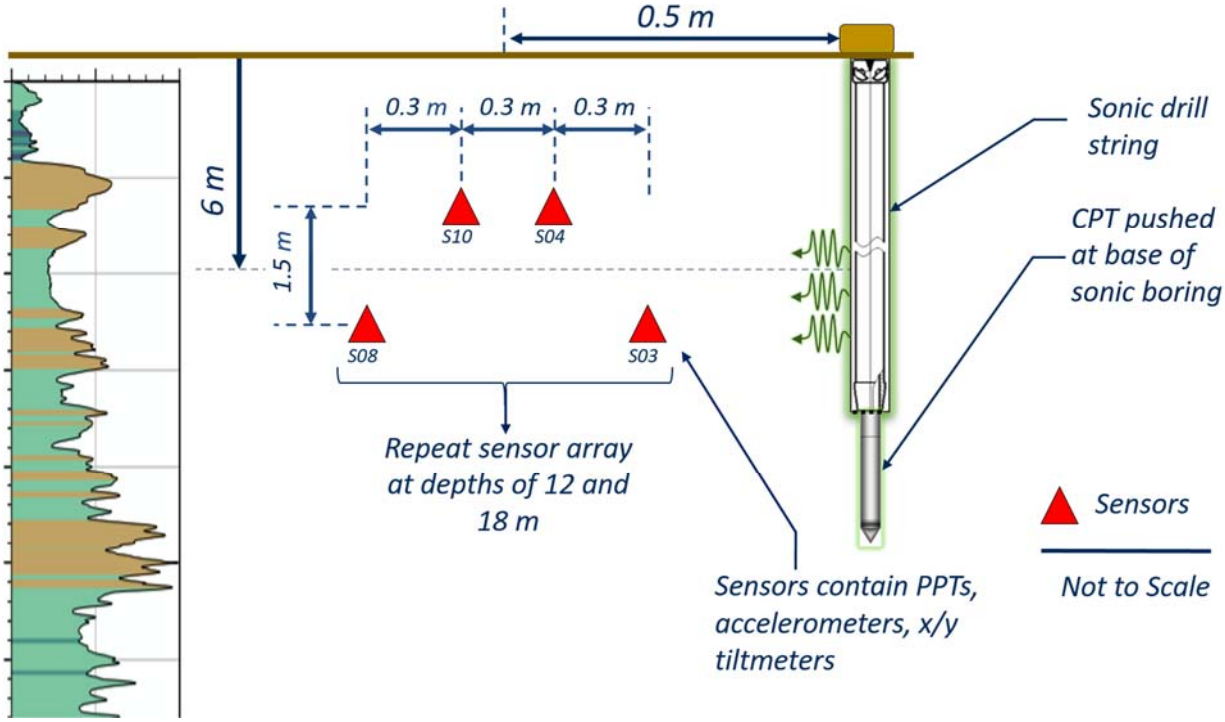

Figure 15 – Phase II testing layout, (a) plan view and (b) profile view.

Figure 16 – Phase II stickup of cone rods attached to SonicWands. The central four SonicWands are covered by the wooden plate.

Figure 17 – Phase II rig lining up over the first boring. The SonicWands are to the right and the DAS is under the white tent.

Figure 18 – CPT truck set up over a cased sonic borehole pushing a post-sonic CPT.

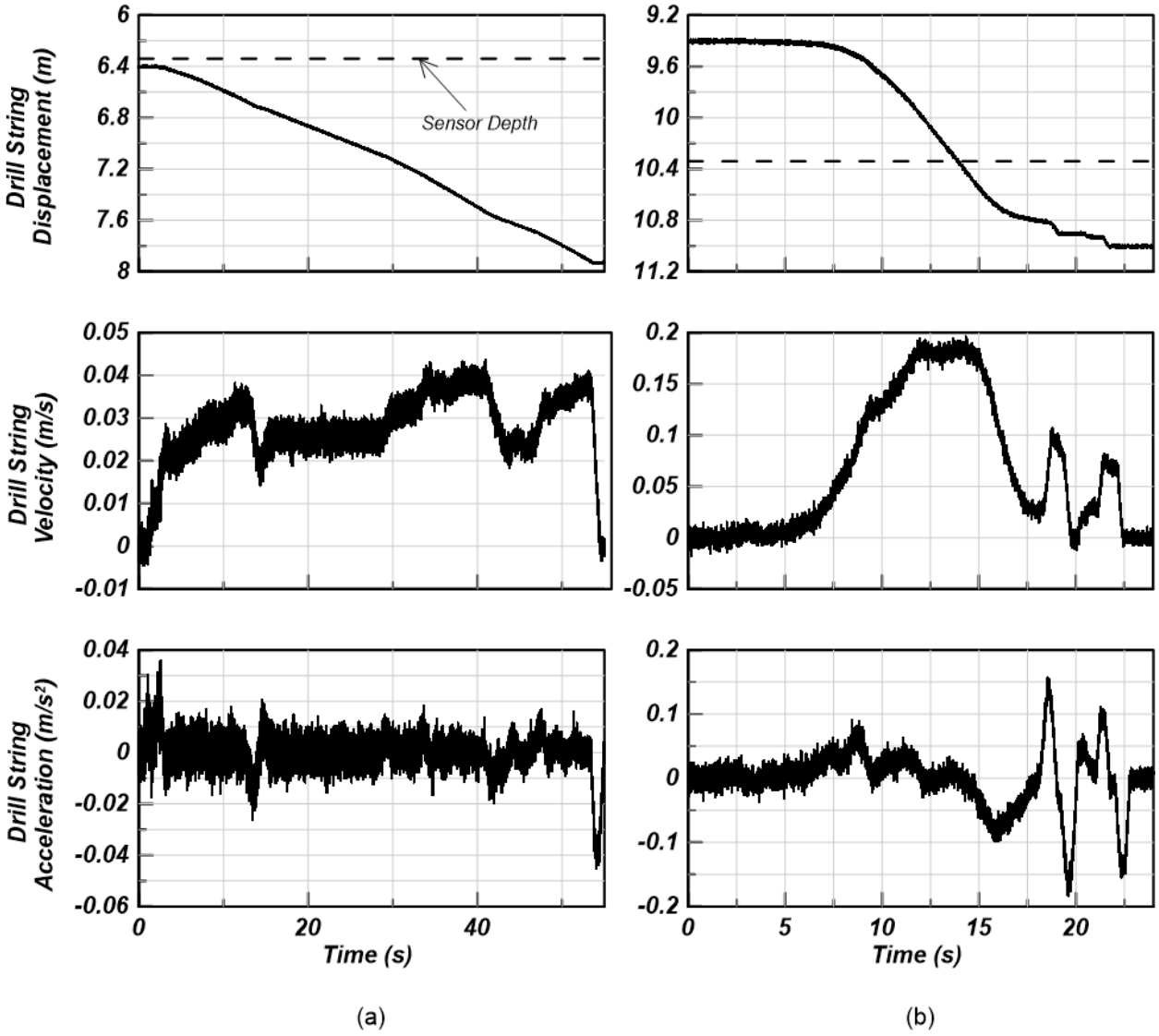

Figure 19 – Phase I displacement, velocity, and acceleration of the drill string for (a) Run 1A and (b) Run 1B.

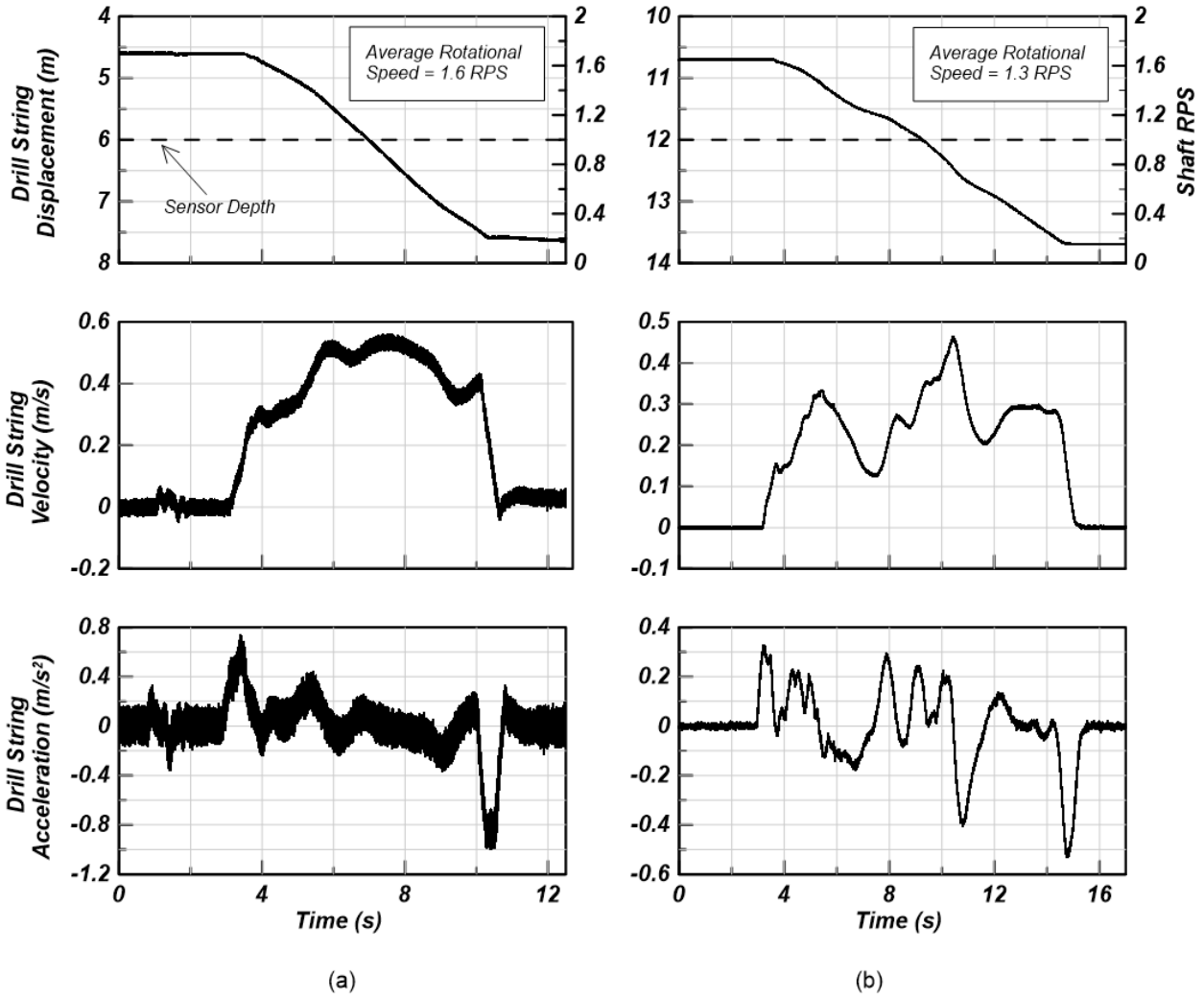

Figure 20 – Phase II displacement, velocity, acceleration and rotational speed of the drill string for (a) Run 2A and (b) Run 2B.

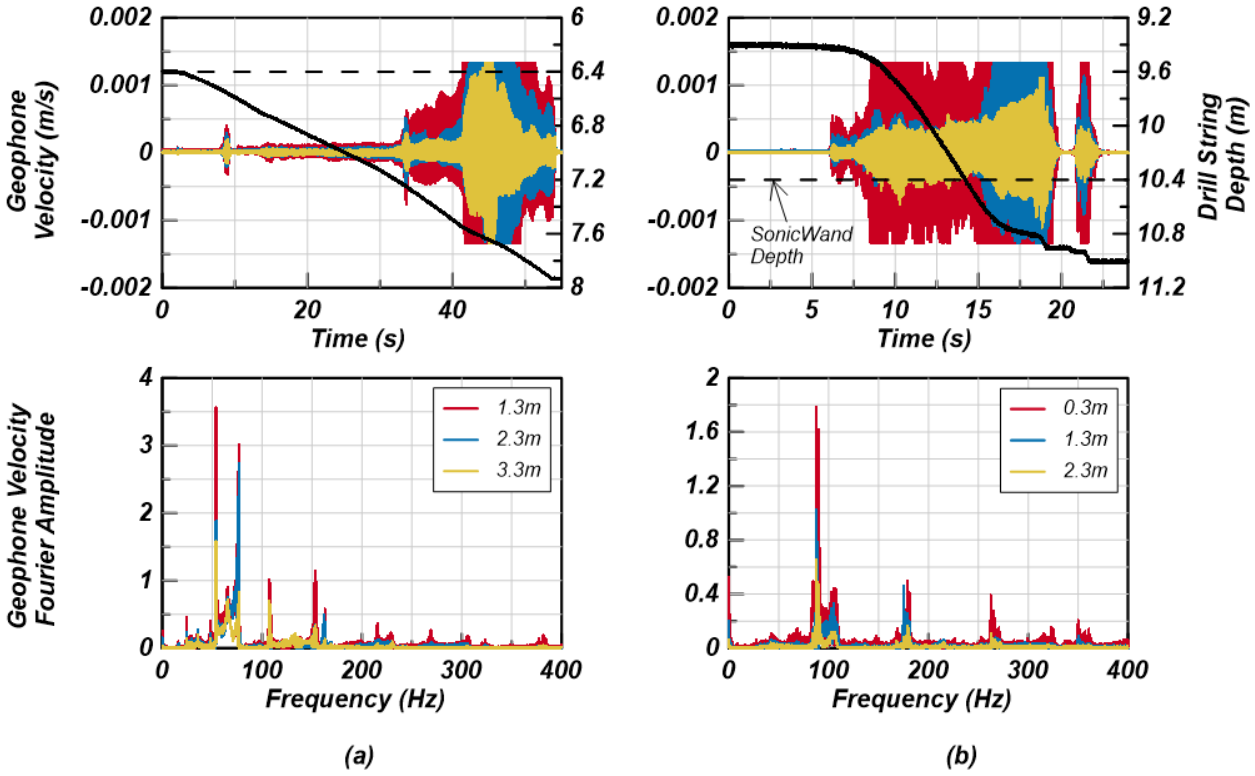

Figure 21 – Phase I X velocity time history and Fourier amplitude spectrum recorded during (a) Run 1A and (b) Run 1B.

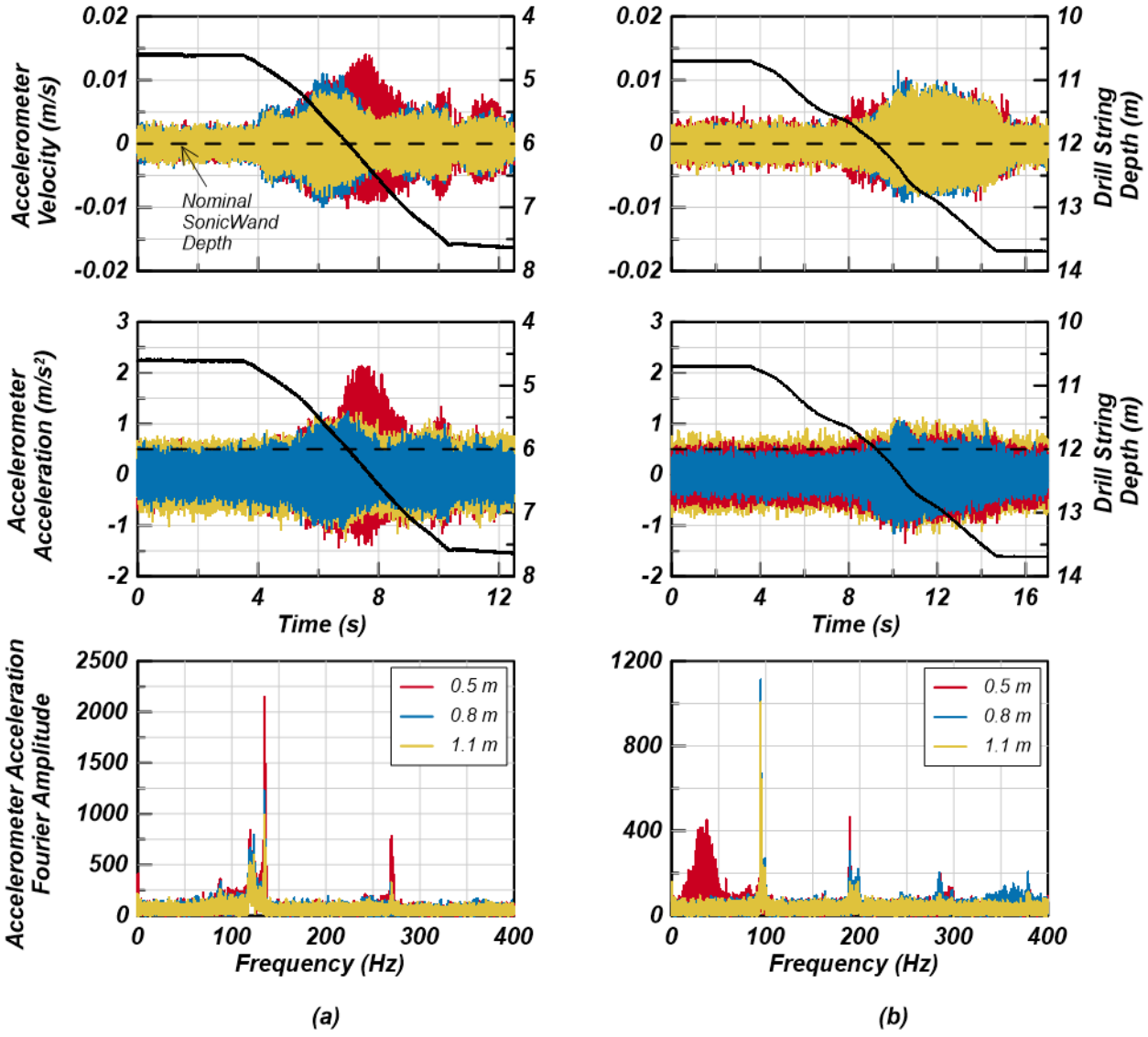

Figure 22 – Phase II X acceleration and velocity time histories and Fourier amplitude spectrum during (a) Run 2A and (b) Run 2B.

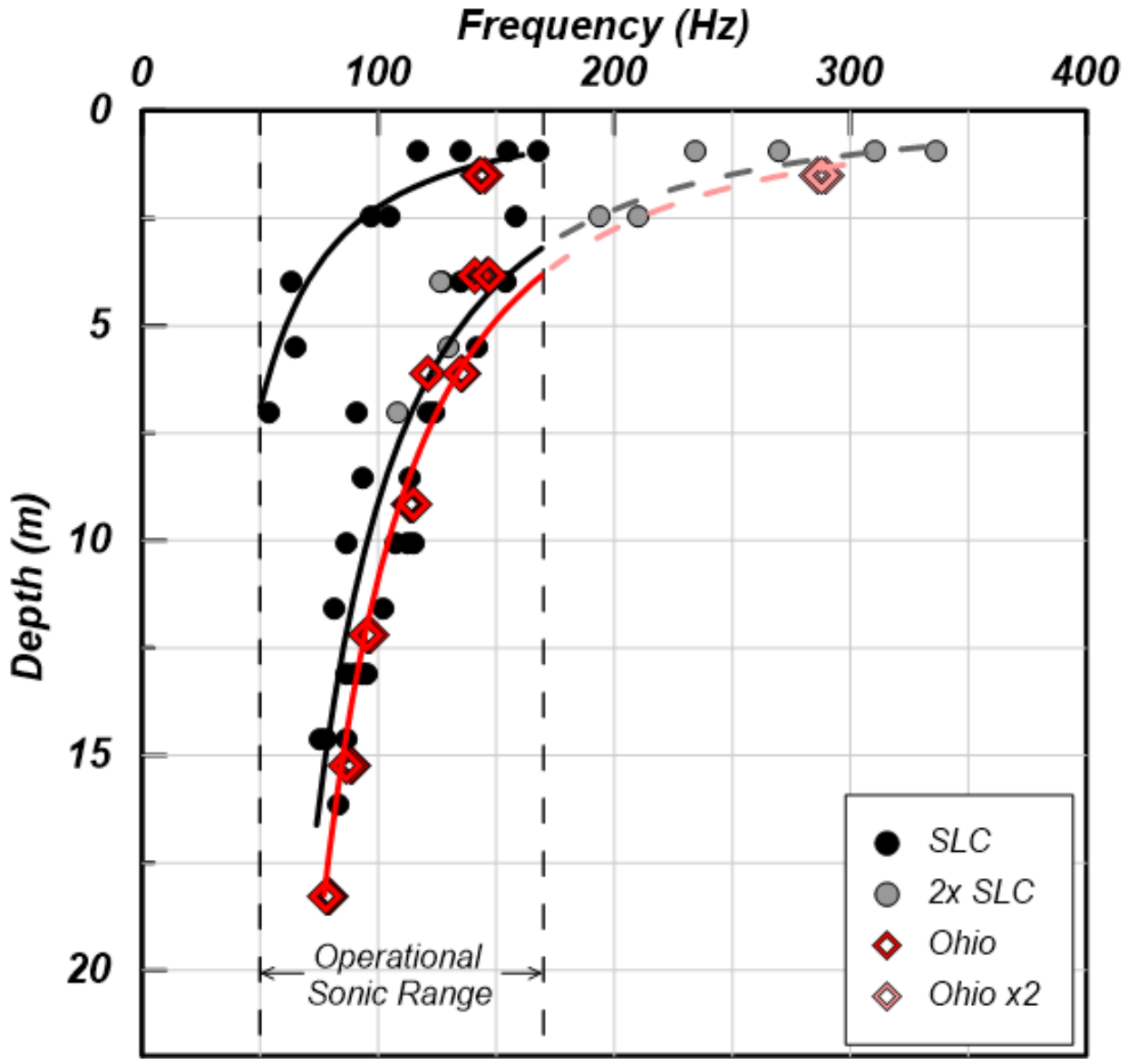

Figure 23 – Relationship between frequency of a drill run and average drill run depth. The light points of each color indicate 2x the measured value at a given depth. This shows the expected frequency at shallower depths where the fundamental system resonance is outside the operational range.

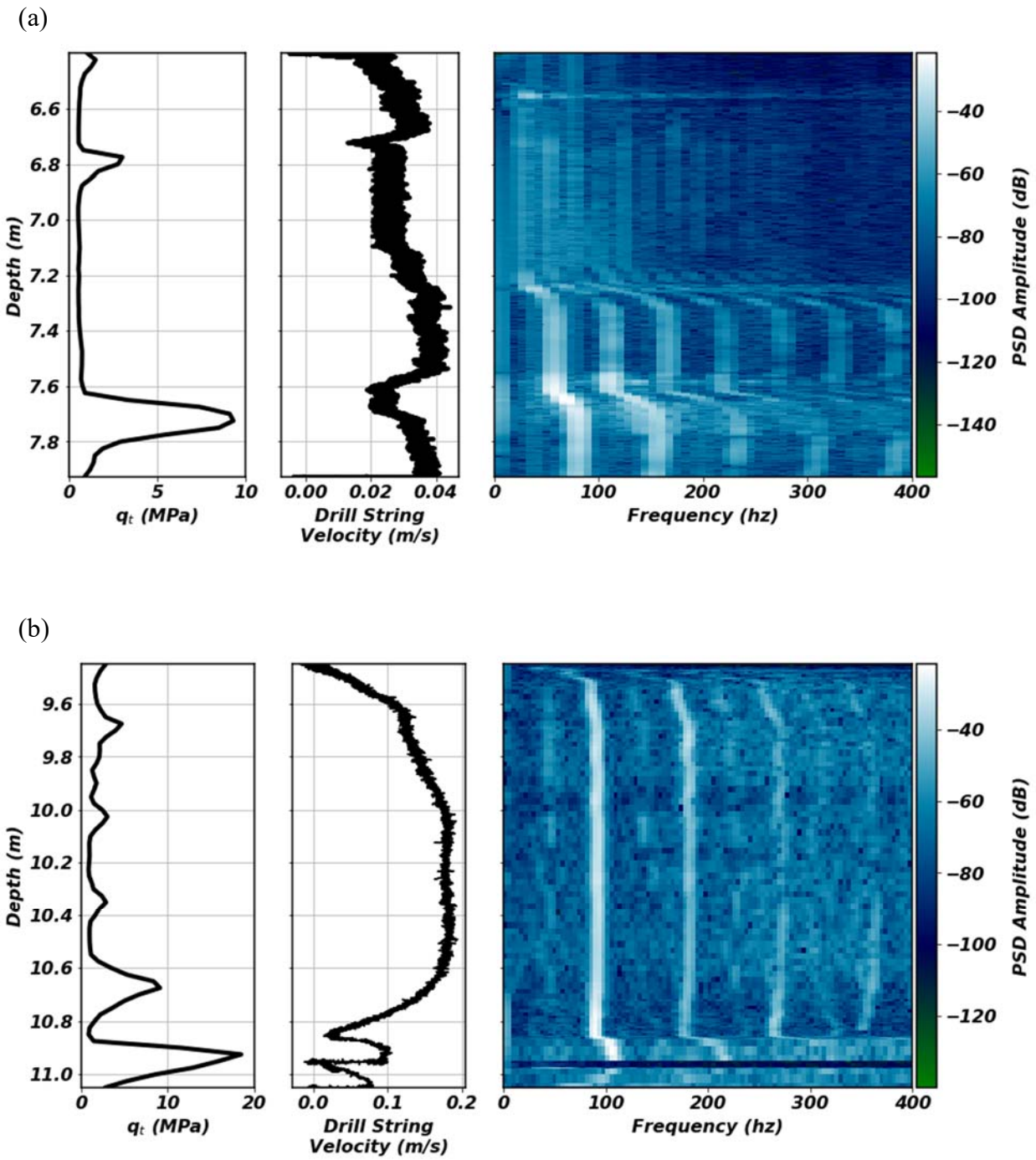

Figure 24 – q_t from CPT7 (Phase I), drill string velocity and X geophone spectrogram for (a) Run 1A and (b) Run 1B.

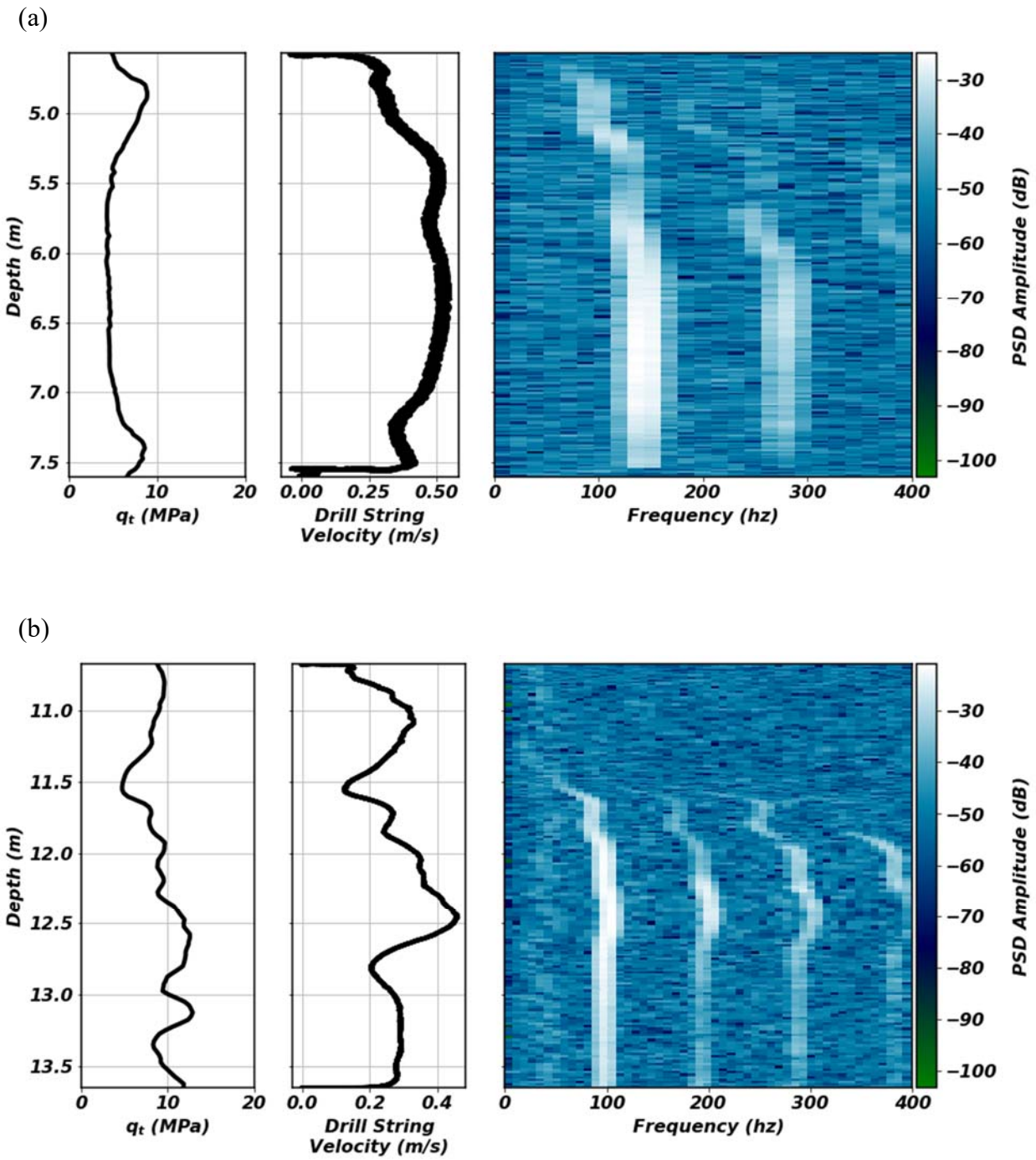

Figure 25 – q_t from CPT5 (Phase II), drill string velocity and X geophone spectrogram for (a) Run 2A and (b) Run 2B.

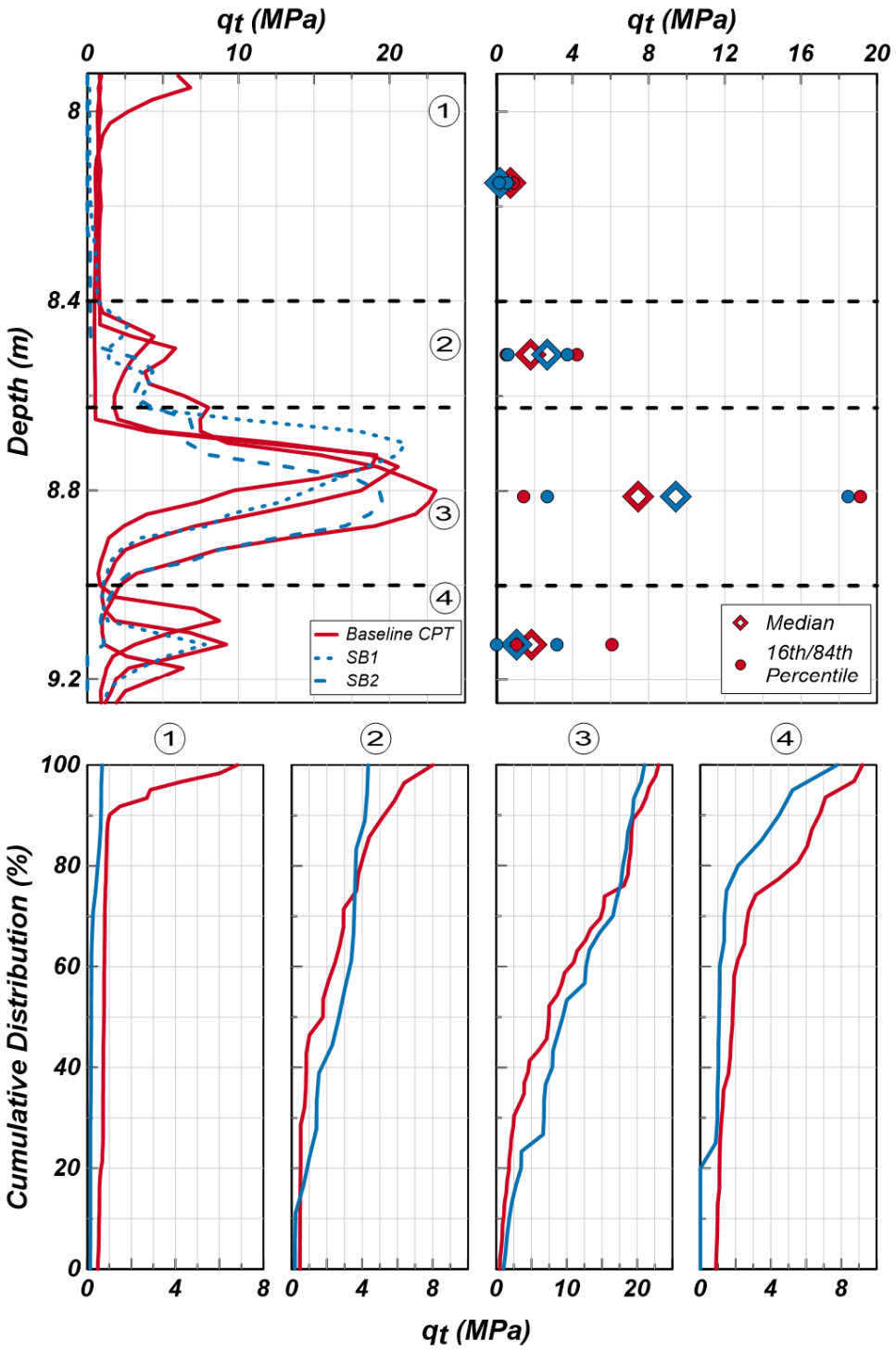

Figure 26 – Phase I baseline/post-sonic CPT comparisons. Baselines are CPT 2, 5, 7.

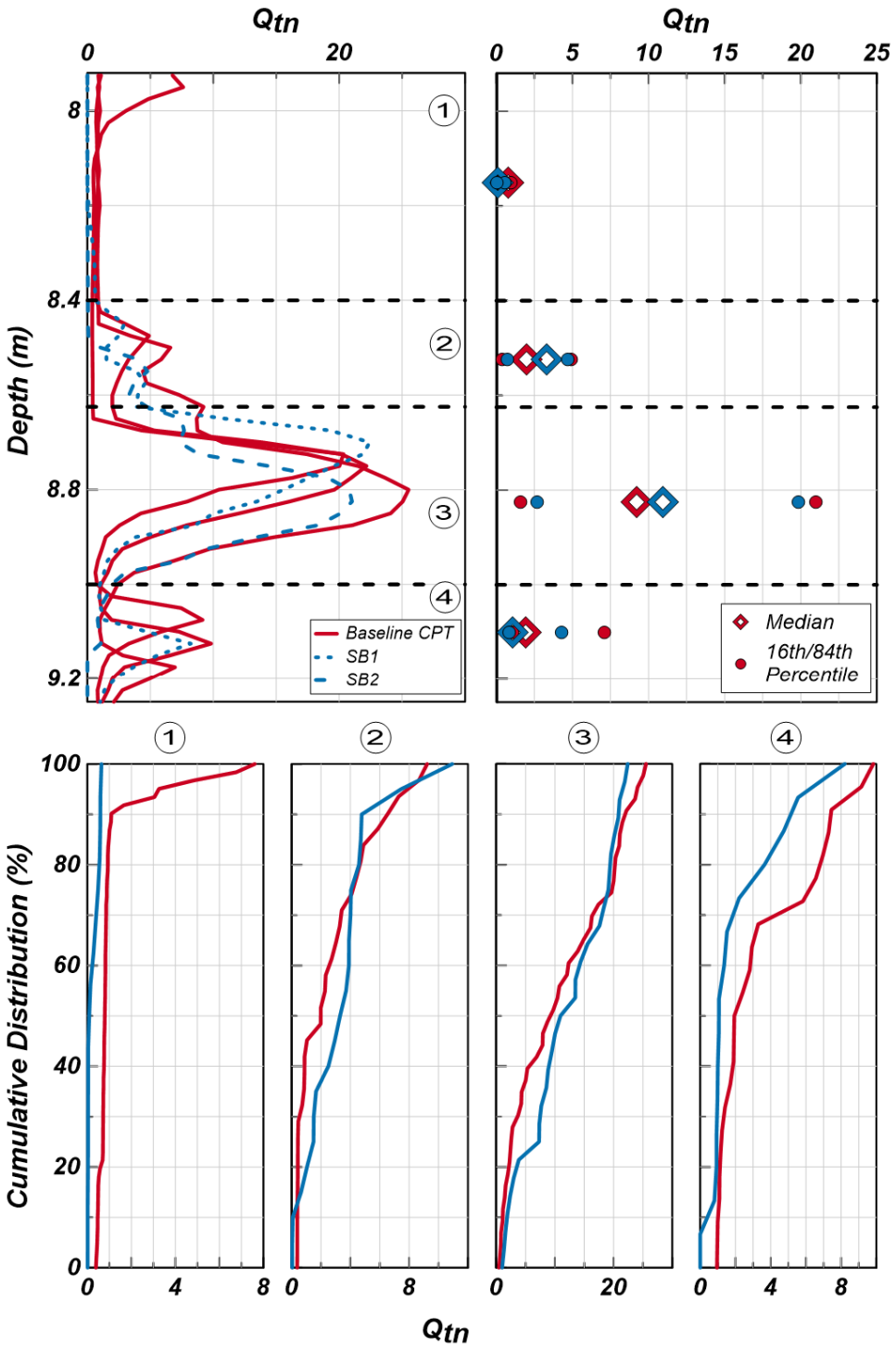

Figure 27 – Phase I baseline/post-sonic CPT comparisons (Q_{tn}). Baselines are CPT 2, 5, 7.

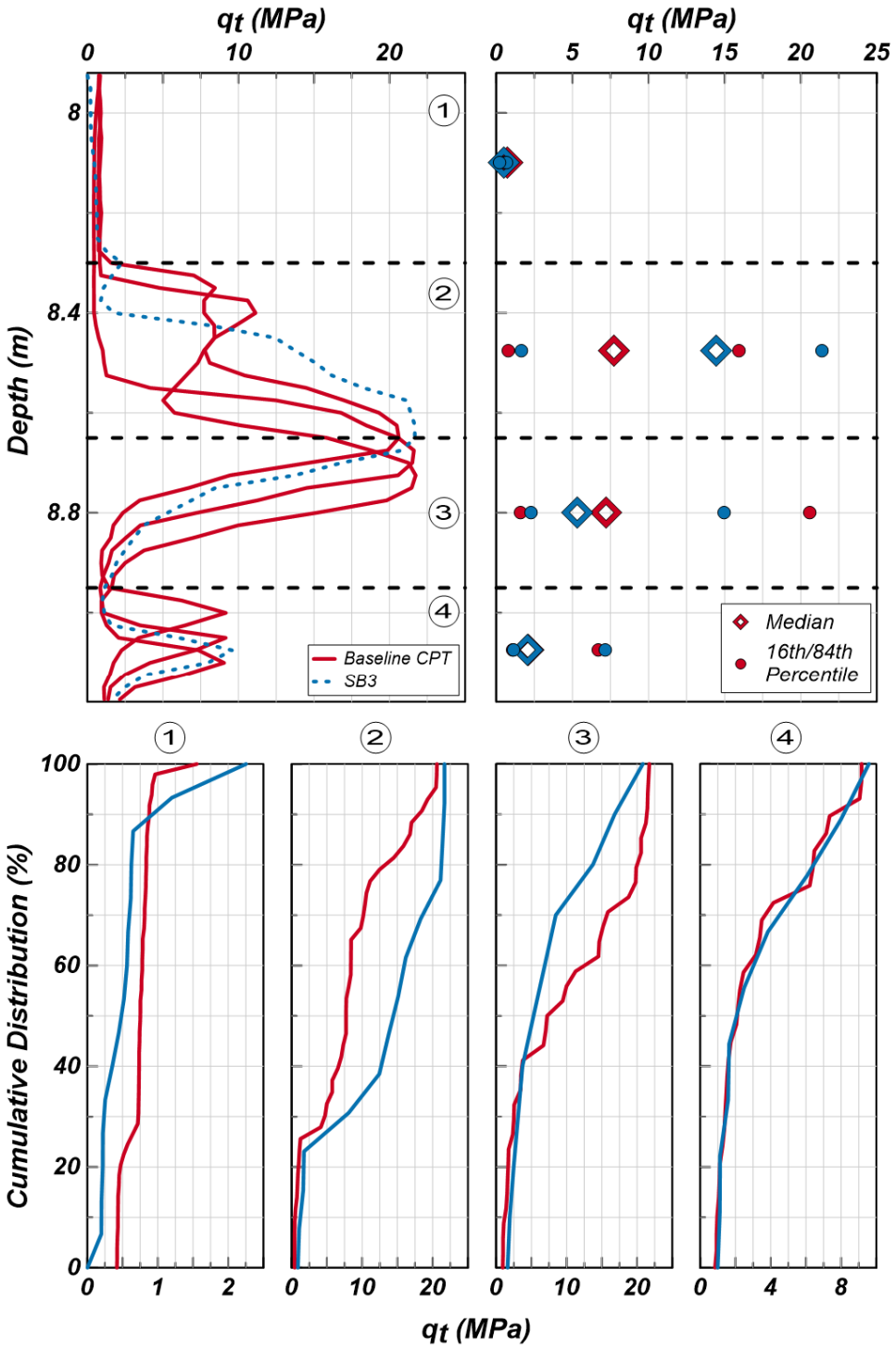

Figure 28 – Phase I baseline/post-sonic CPT comparisons. Baselines are CPT 1, 3, 6.

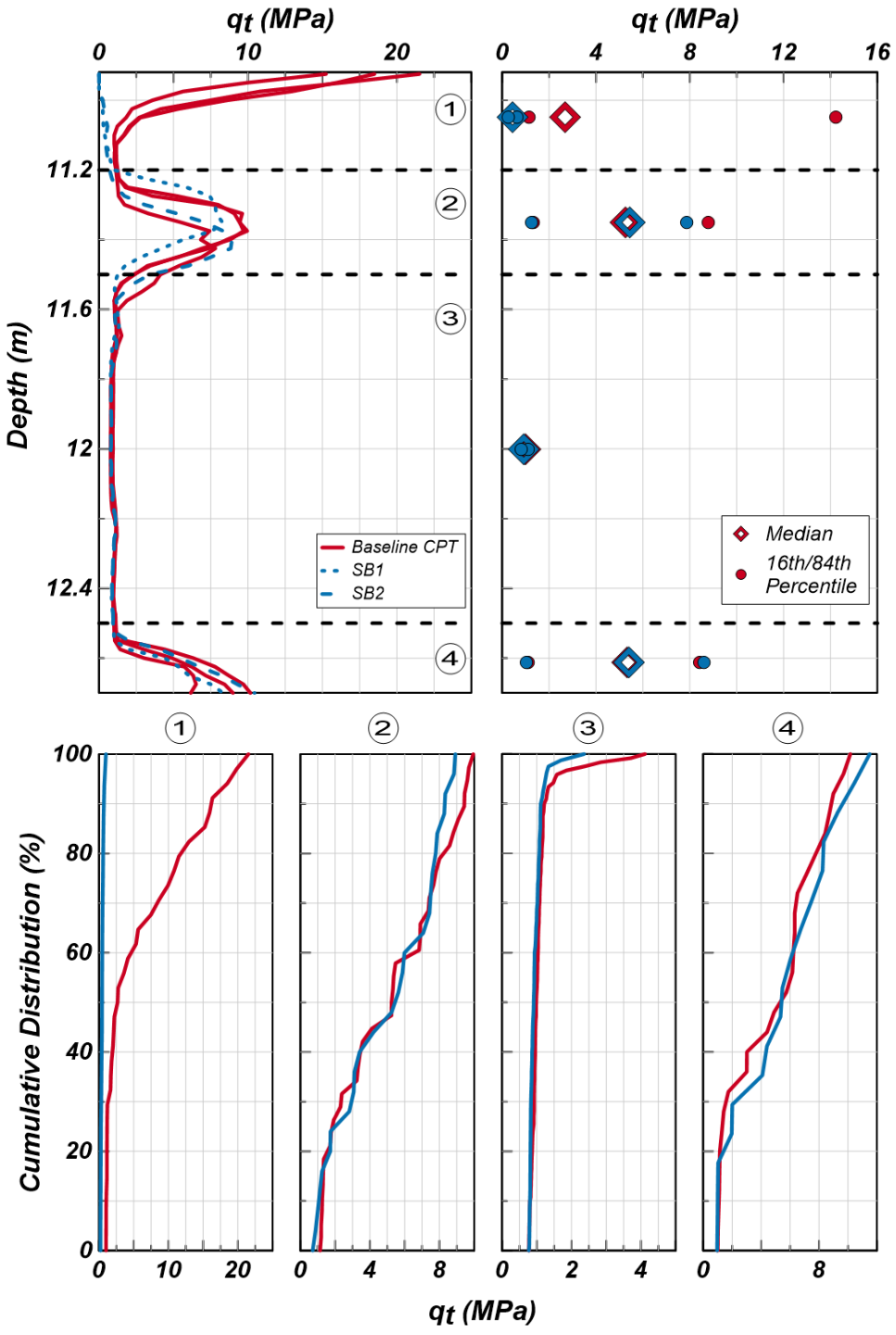

Figure 29 – Phase I baseline/post-sonic CPT comparisons. Baselines are CPT 2, 5, 7.

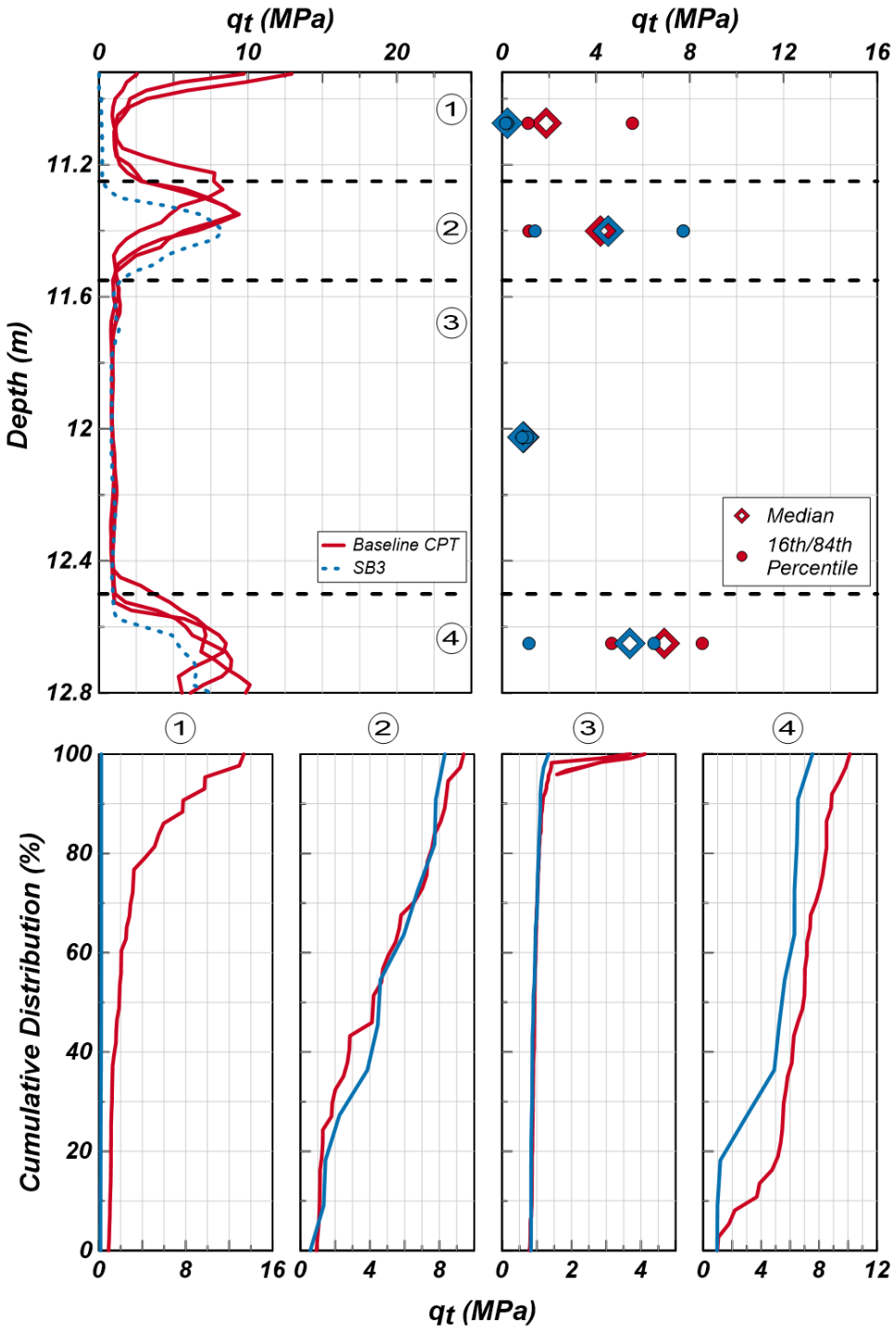

Figure 30 – Phase I baseline/post-sonic CPT comparisons. Baselines are CPT 1, 3, 6.

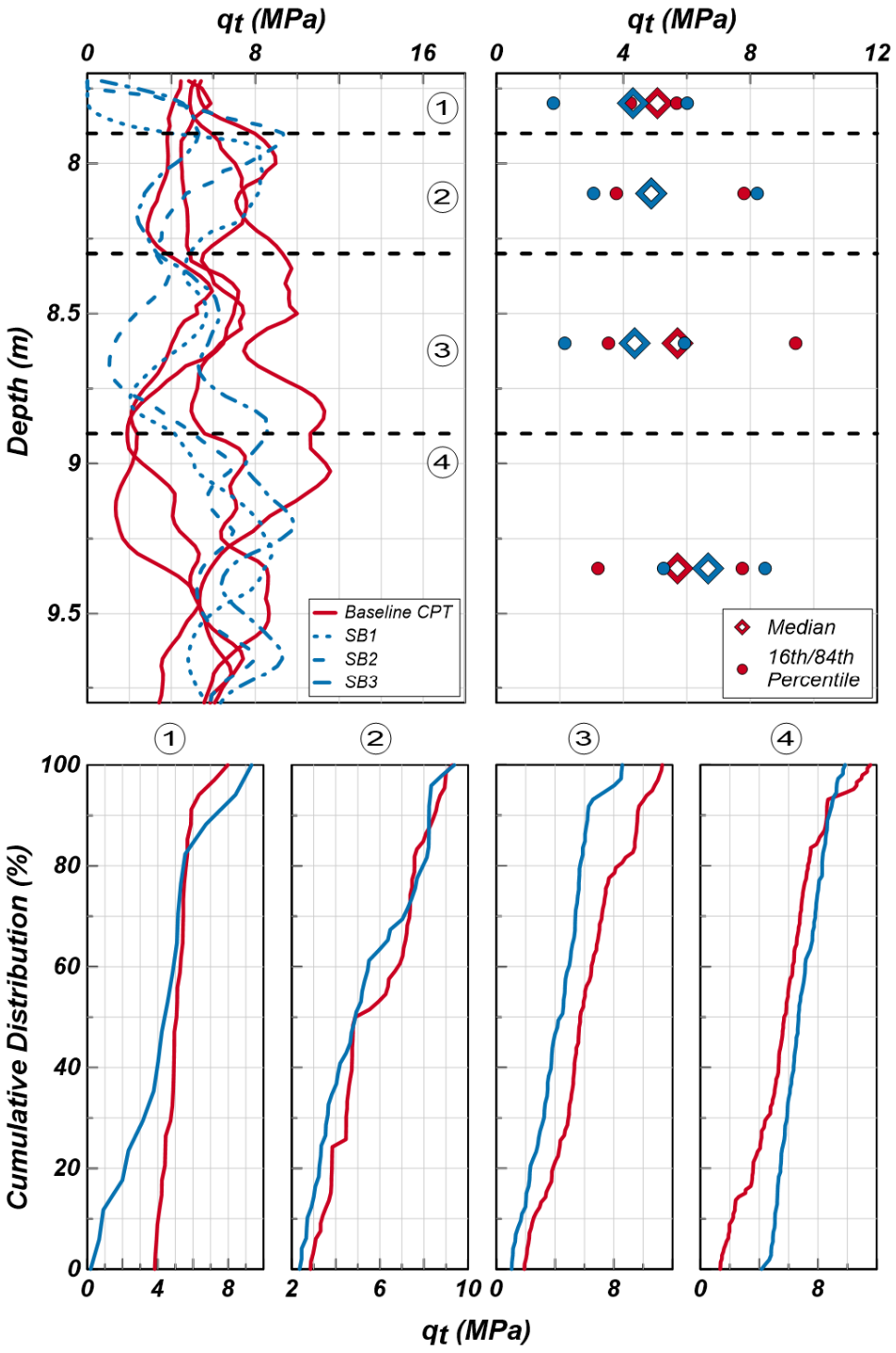

Figure 31 – Phase II baseline/post-sonic CPT comparisons. Baselines are CPT 2, 5, 7, 9.

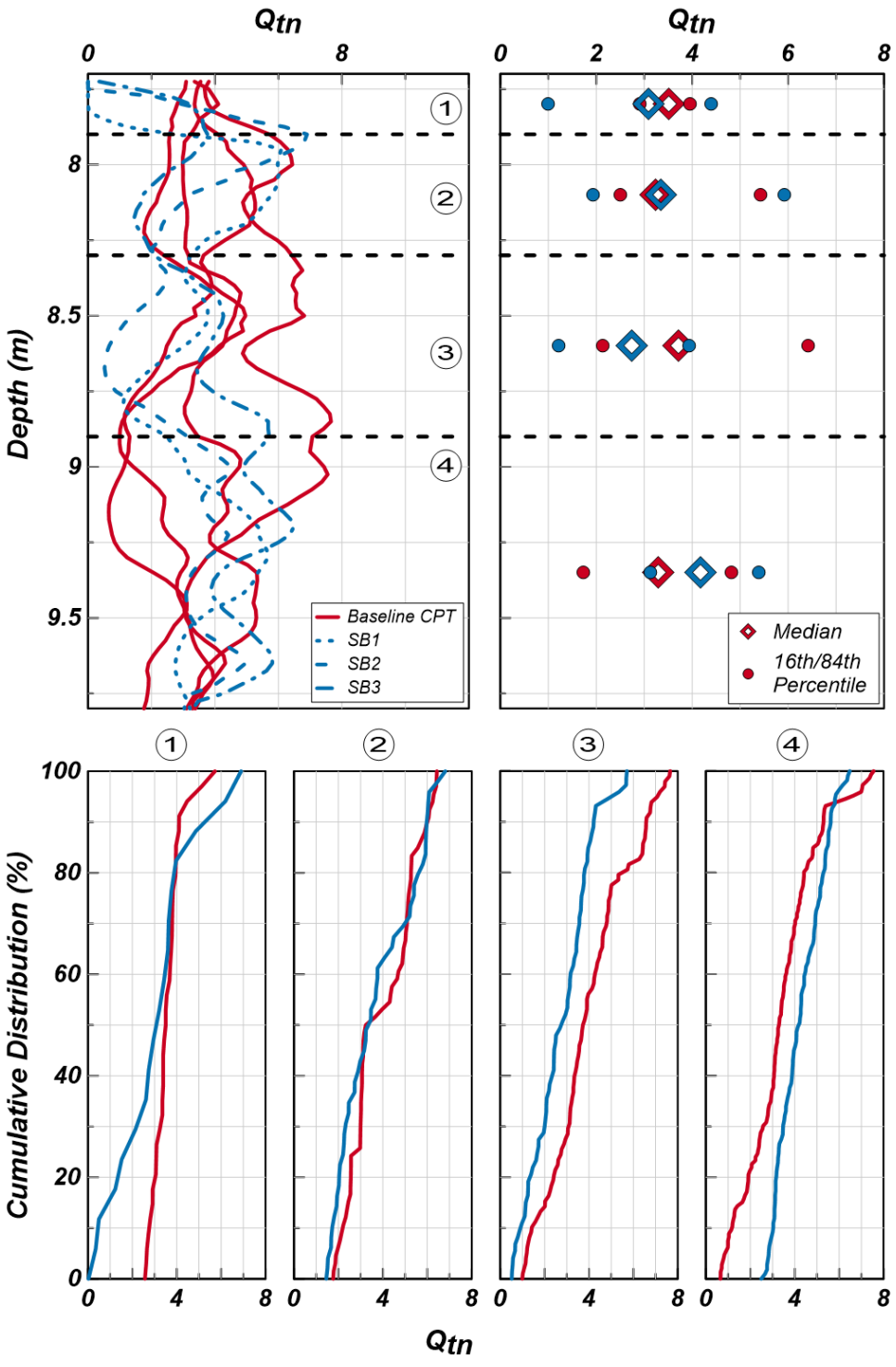

Figure 32 – Phase II baseline/post-sonic CPT comparison (Q_{tn}). Baselines are CPT 2, 5, 7, 9.

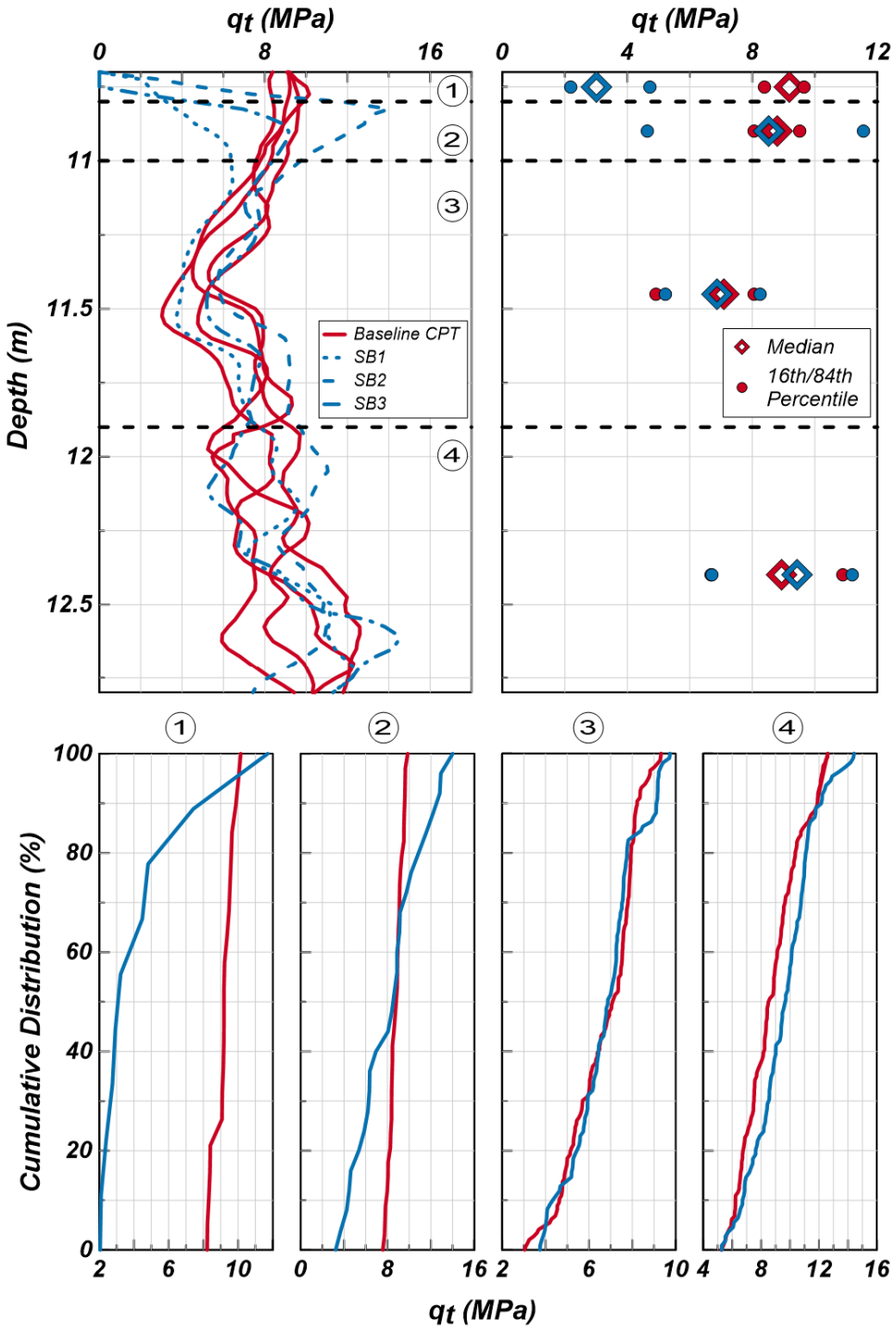

Figure 33 – Phase II baseline/post-sonic CPT comparisons. Baselines are CPT 2, 5, 7, 9.

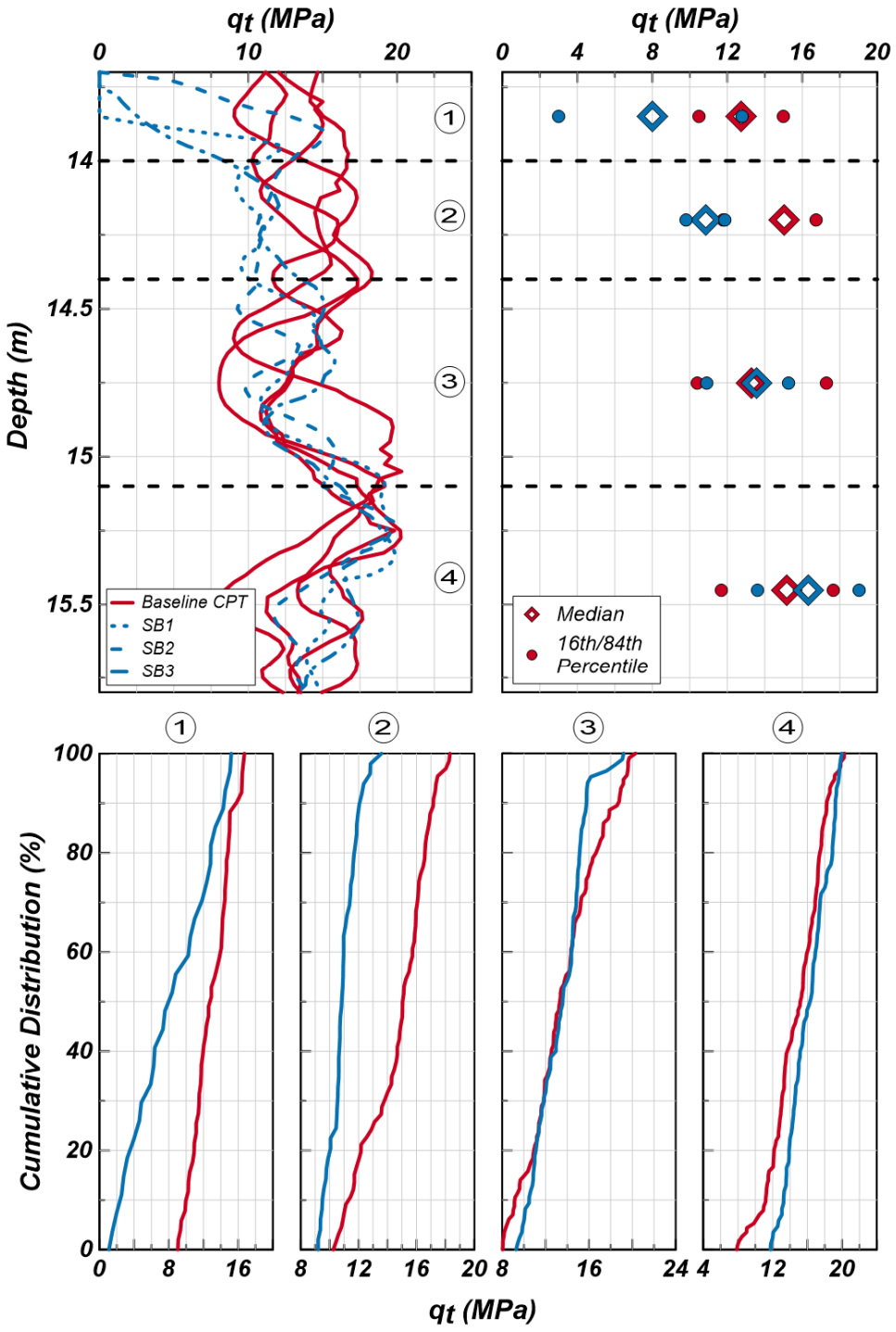

Figure 34 – Phase II baseline/post-sonic CPT comparisons. Baselines are CPT 2, 5, 7, 9.

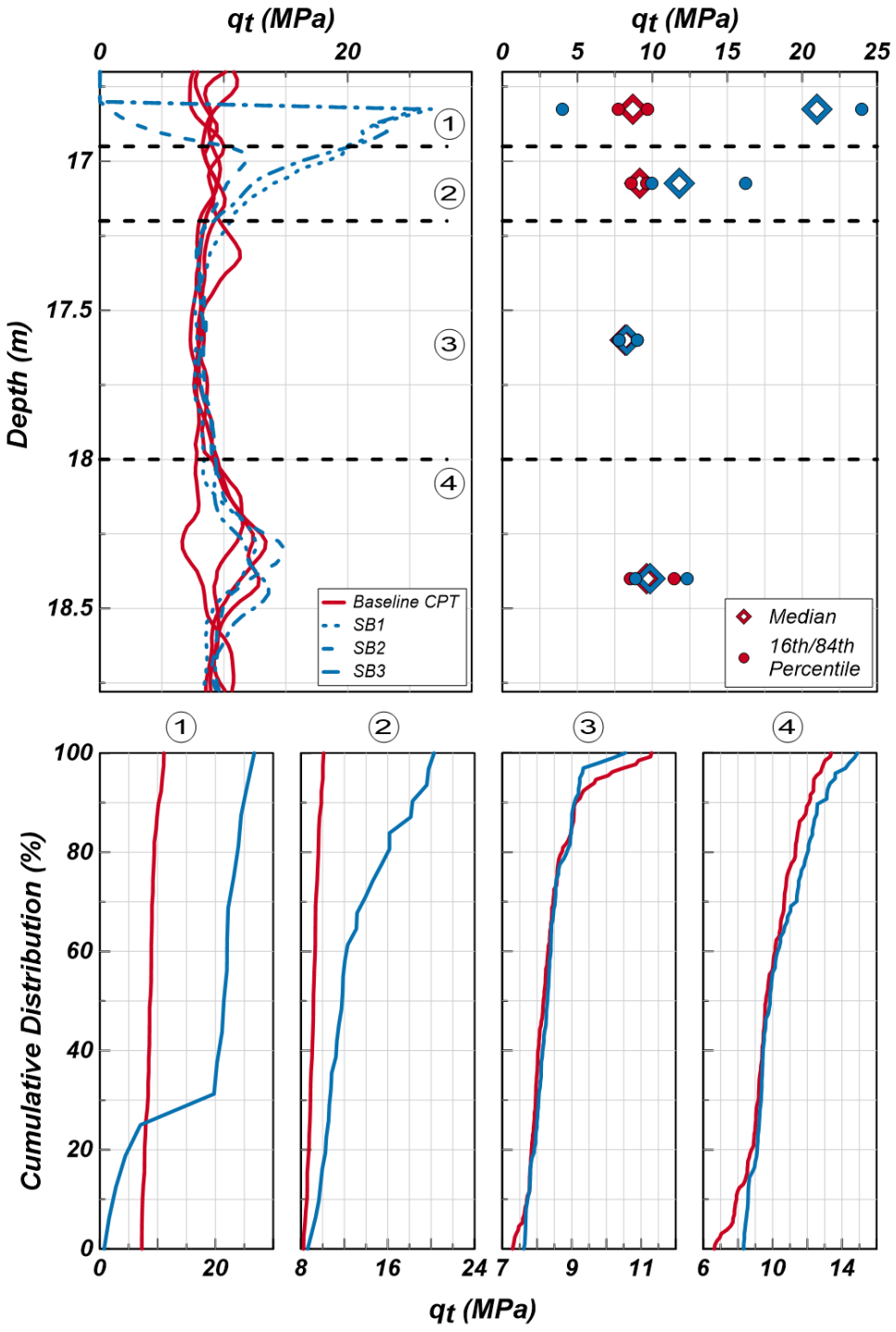

Figure 35 – Phase II baseline/post-sonic CPT comparisons. Baselines are CPT 2, 5, 7, 9.

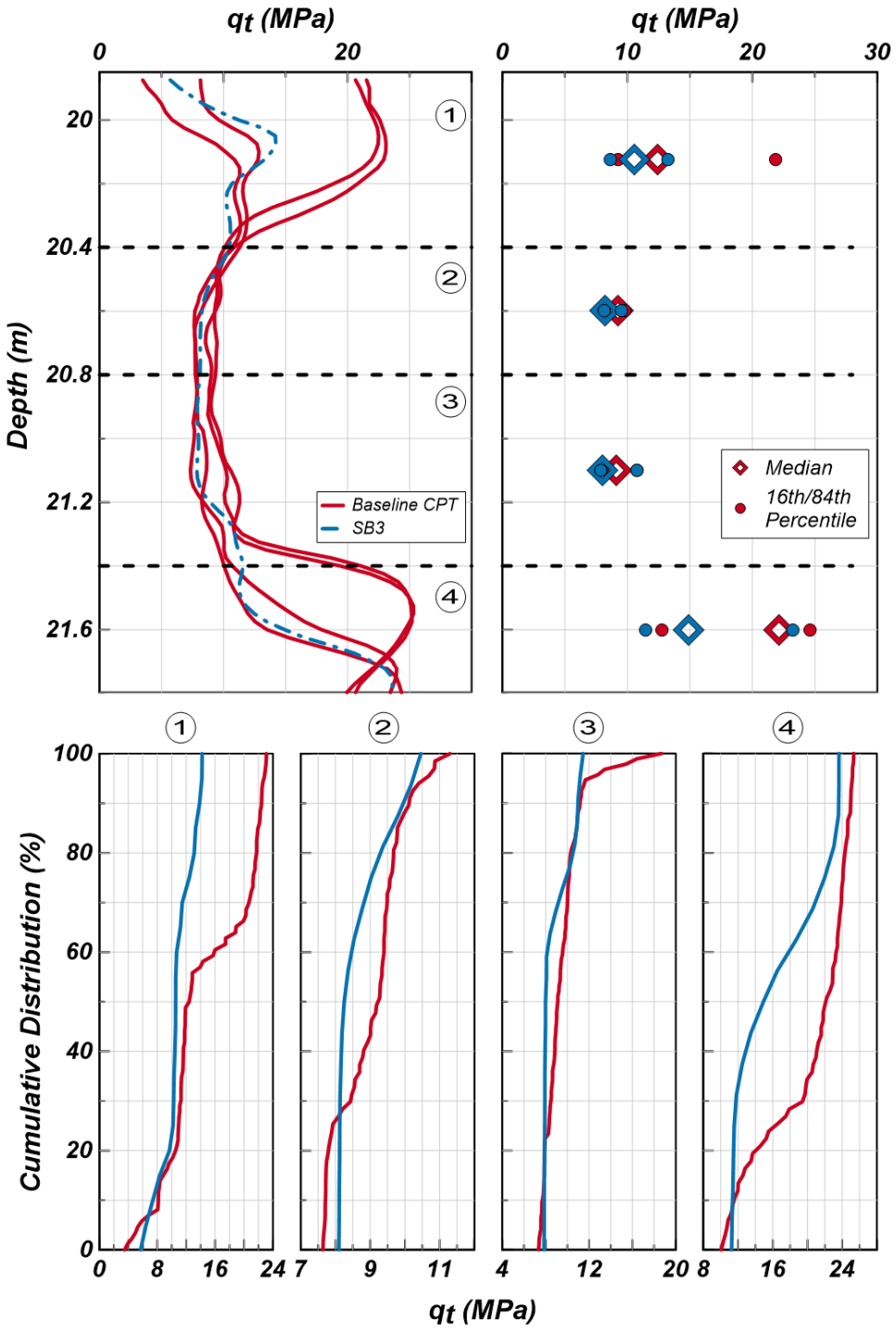

Figure 36 – Phase II baseline/post-sonic CPT comparisons. Baselines are CPT 2, 5, 7, 9.

APPENDIX A – PHASE I TIME HISTORY FIGURES

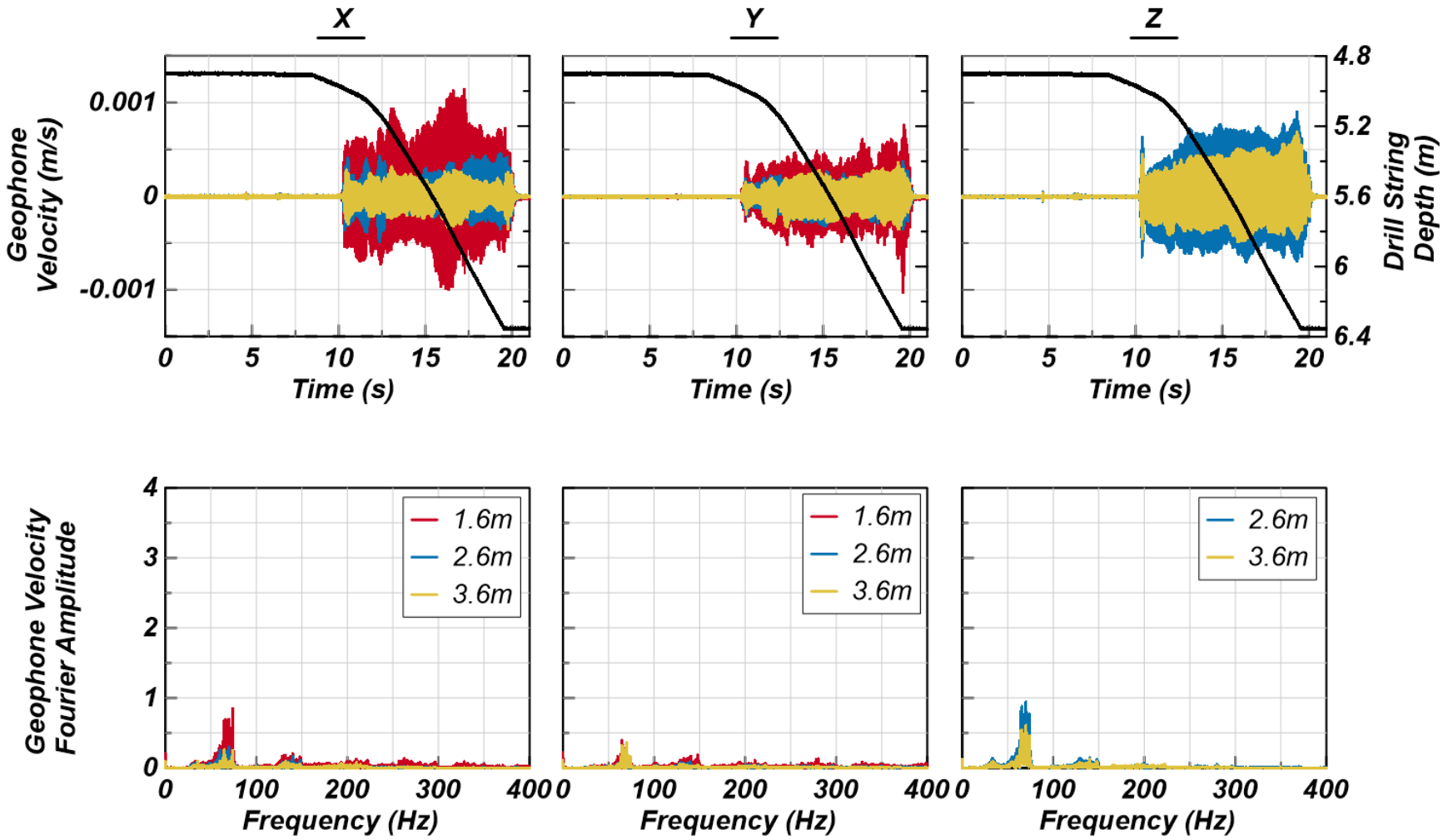

Figure A1 – Phase I velocity time histories and Fourier amplitude spectra recorded during SB1 from 4.9 to 6.4 m.

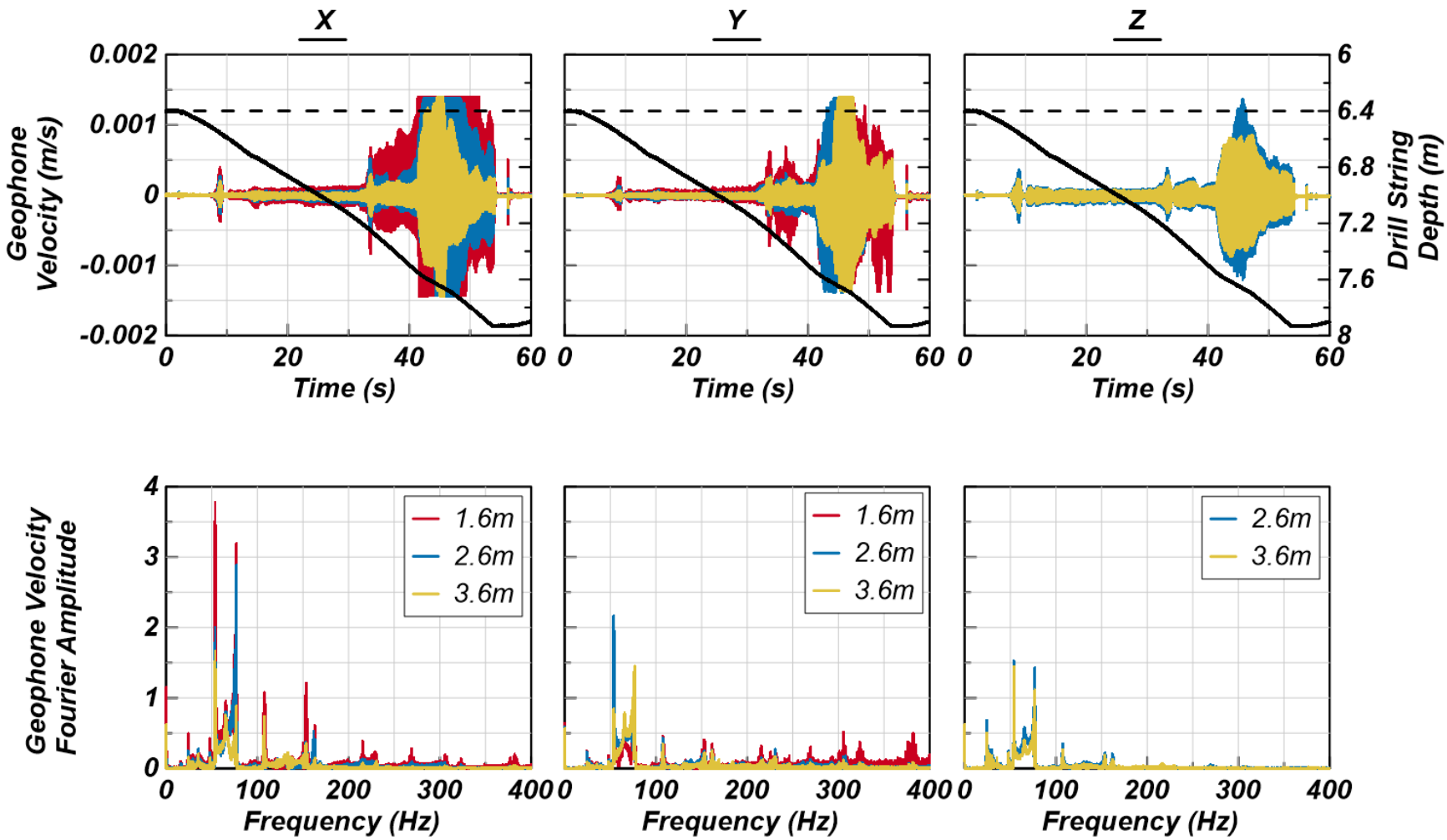

Figure A2 – Phase I velocity time histories and Fourier amplitude spectra recorded during SB1 from 6.4 to 7.9 m.

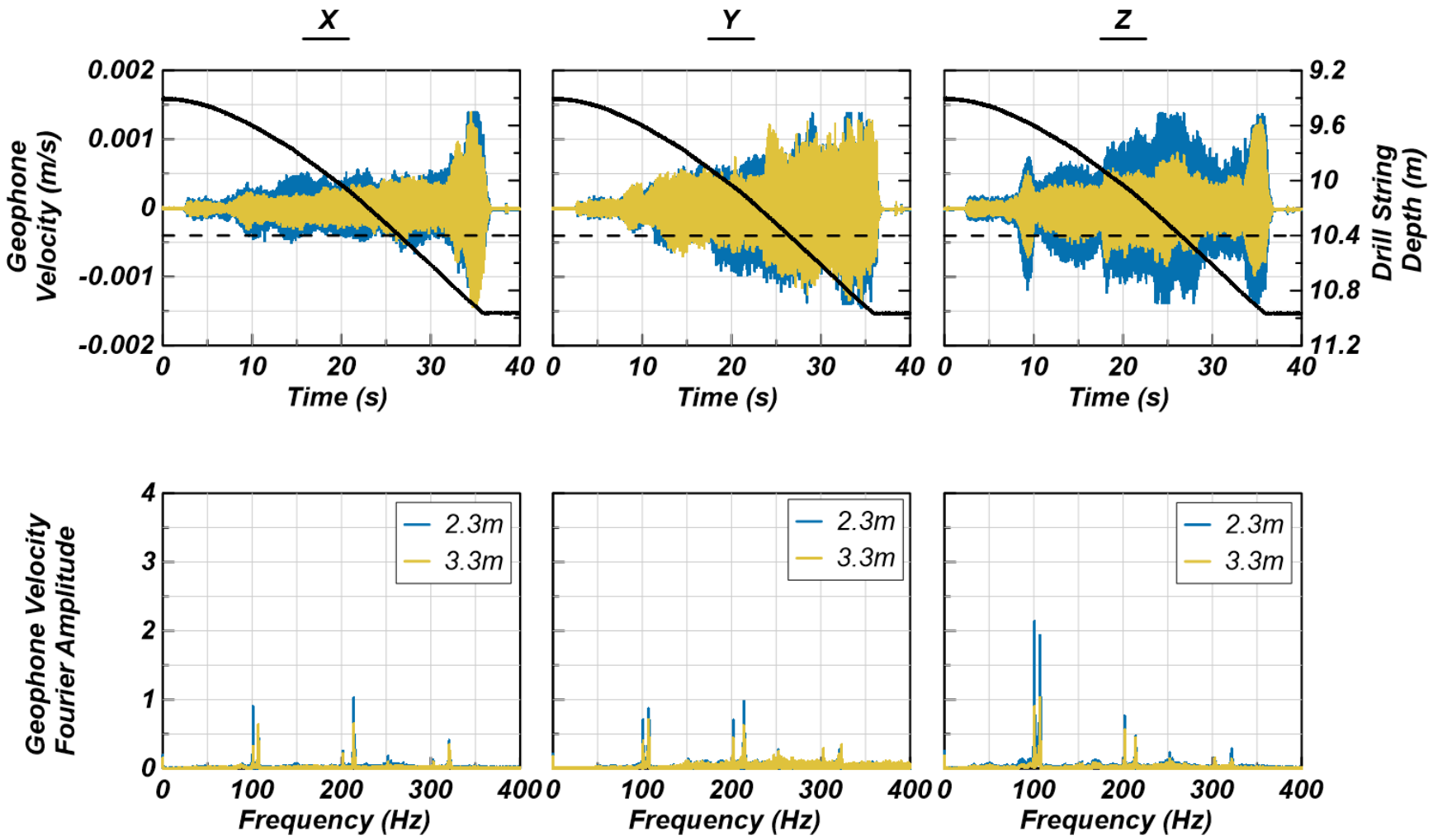

Figure A3 – Phase I velocity time histories and Fourier amplitude spectra recorded during SB1 from 9.4 to 11.0 m.

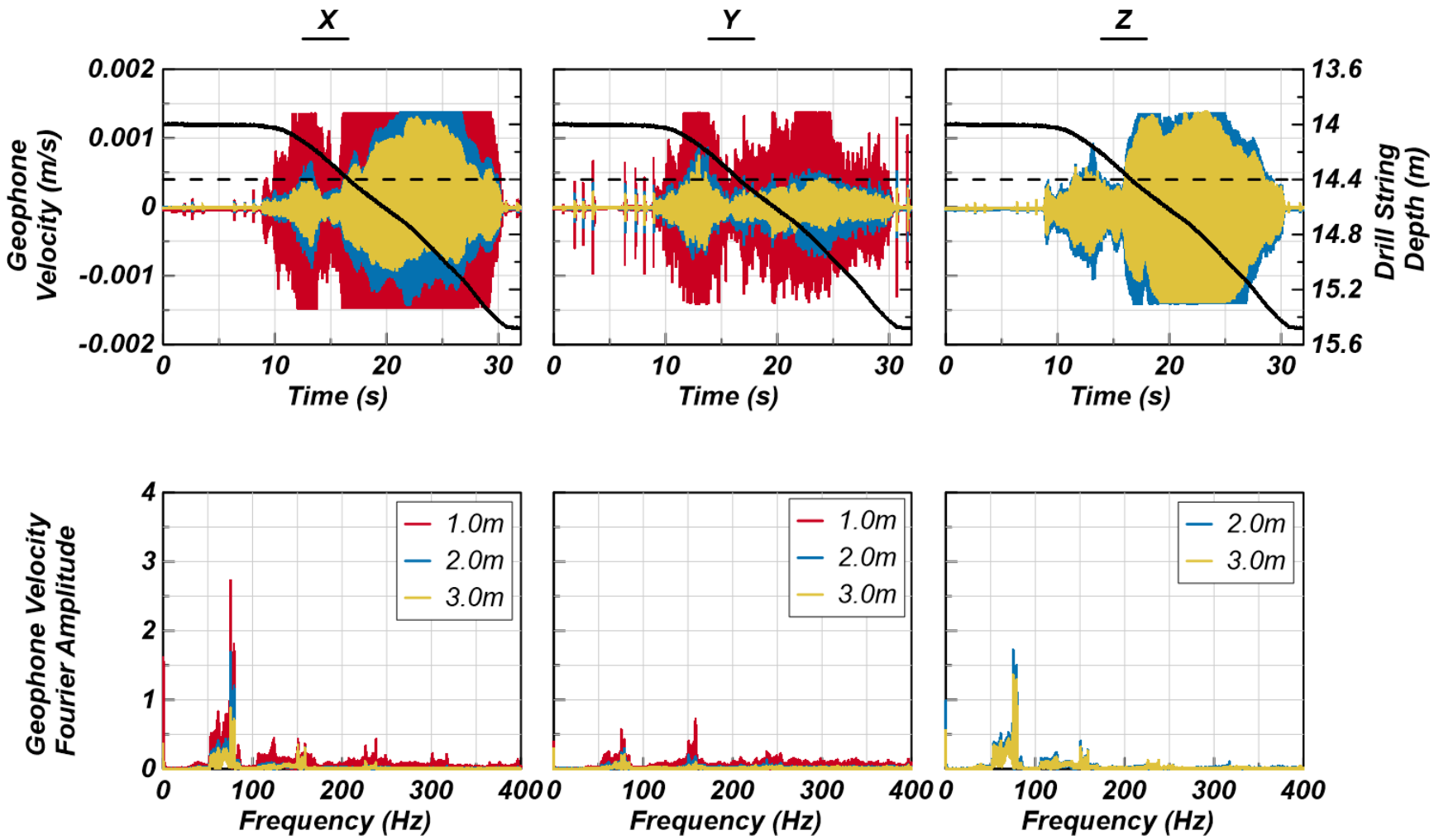

Figure A4 – Phase I velocity time histories and Fourier amplitude spectra recorded during SB1 from 14 to 15.5 m.

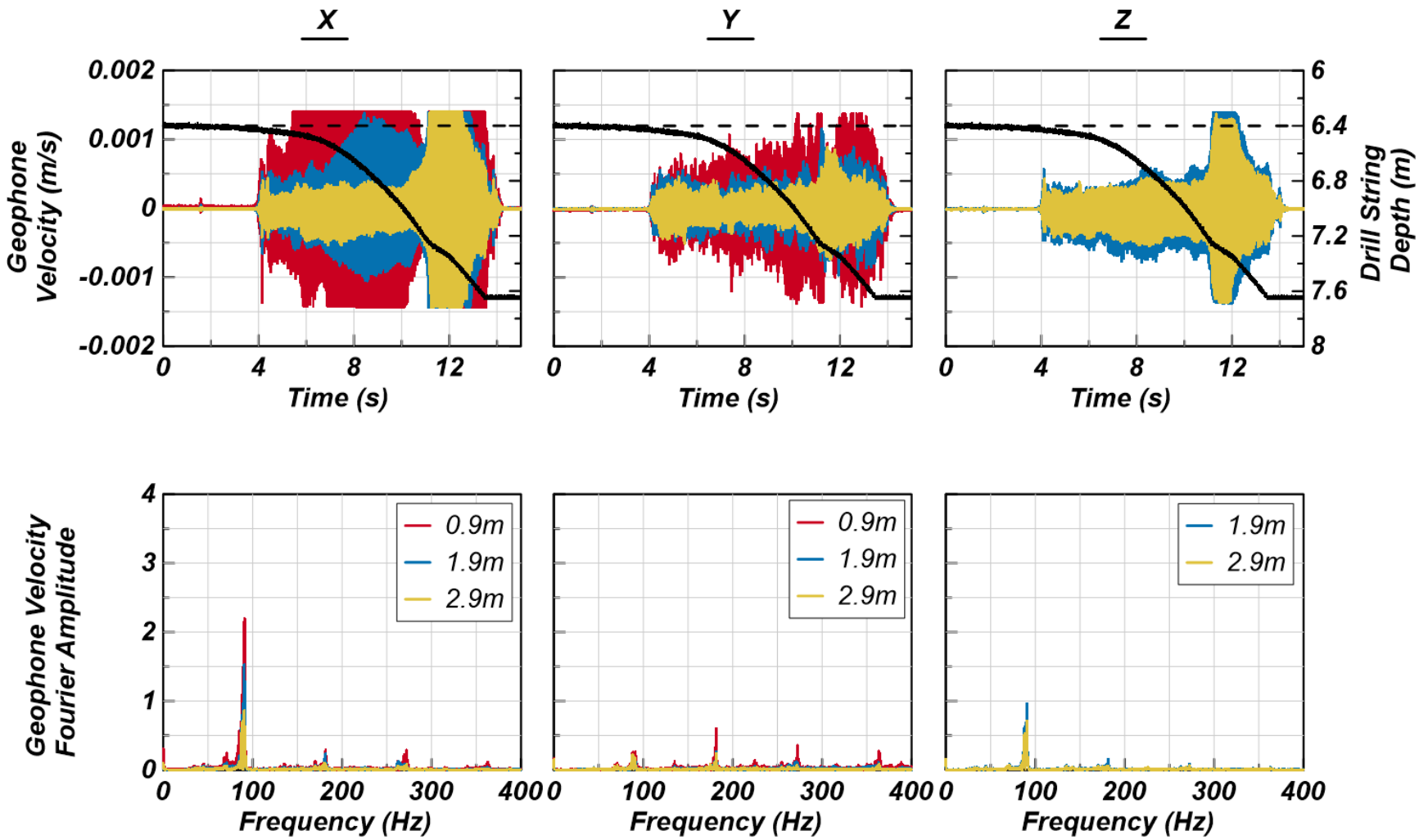

Figure A5 – Phase I velocity time histories and Fourier amplitude spectra recorded during SB2 from 6.4 to 7.6 m.

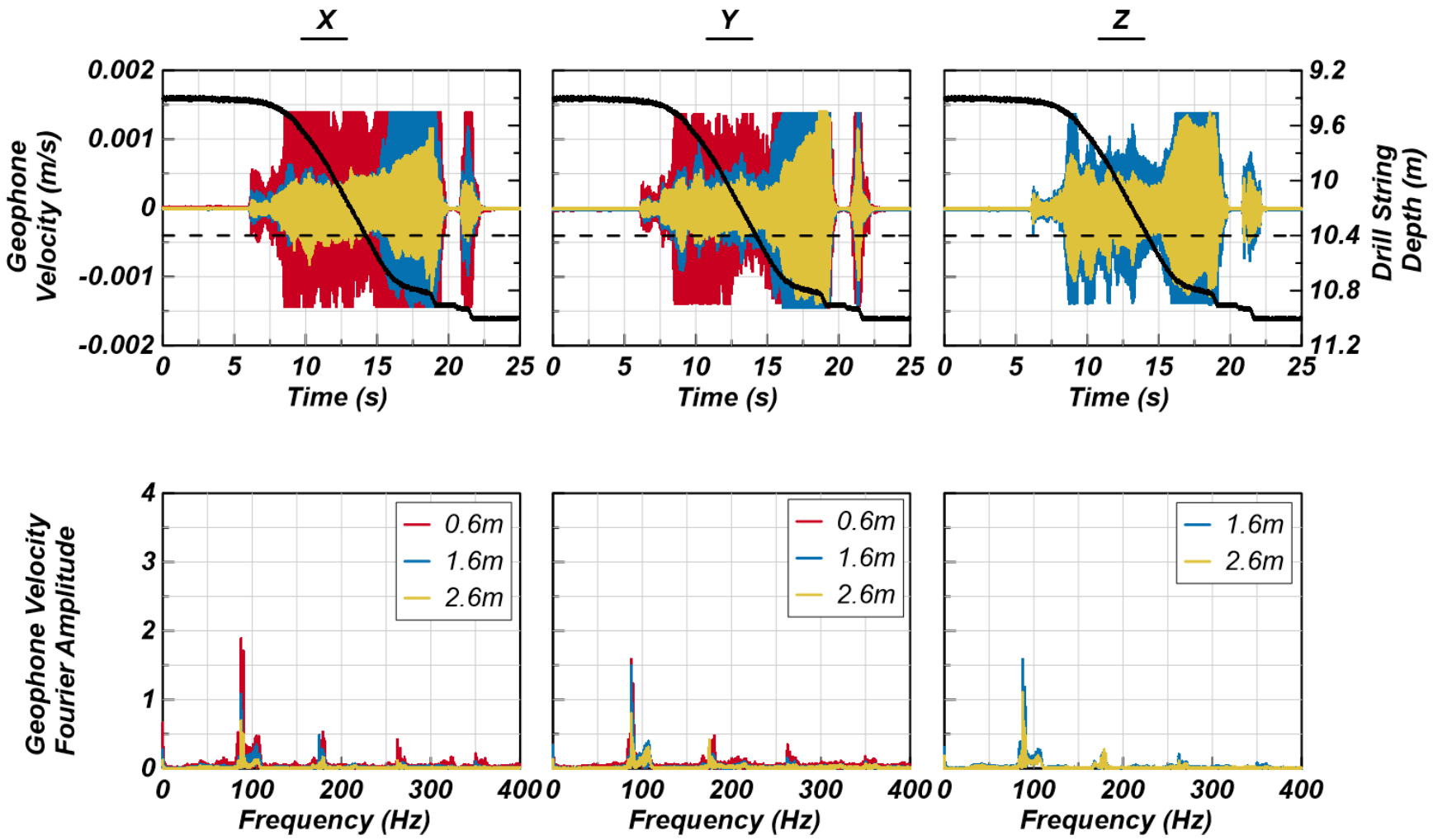

Figure A6 – Phase I velocity time histories and Fourier amplitude spectra recorded during SB2 from 9.4 to 11.0 m.

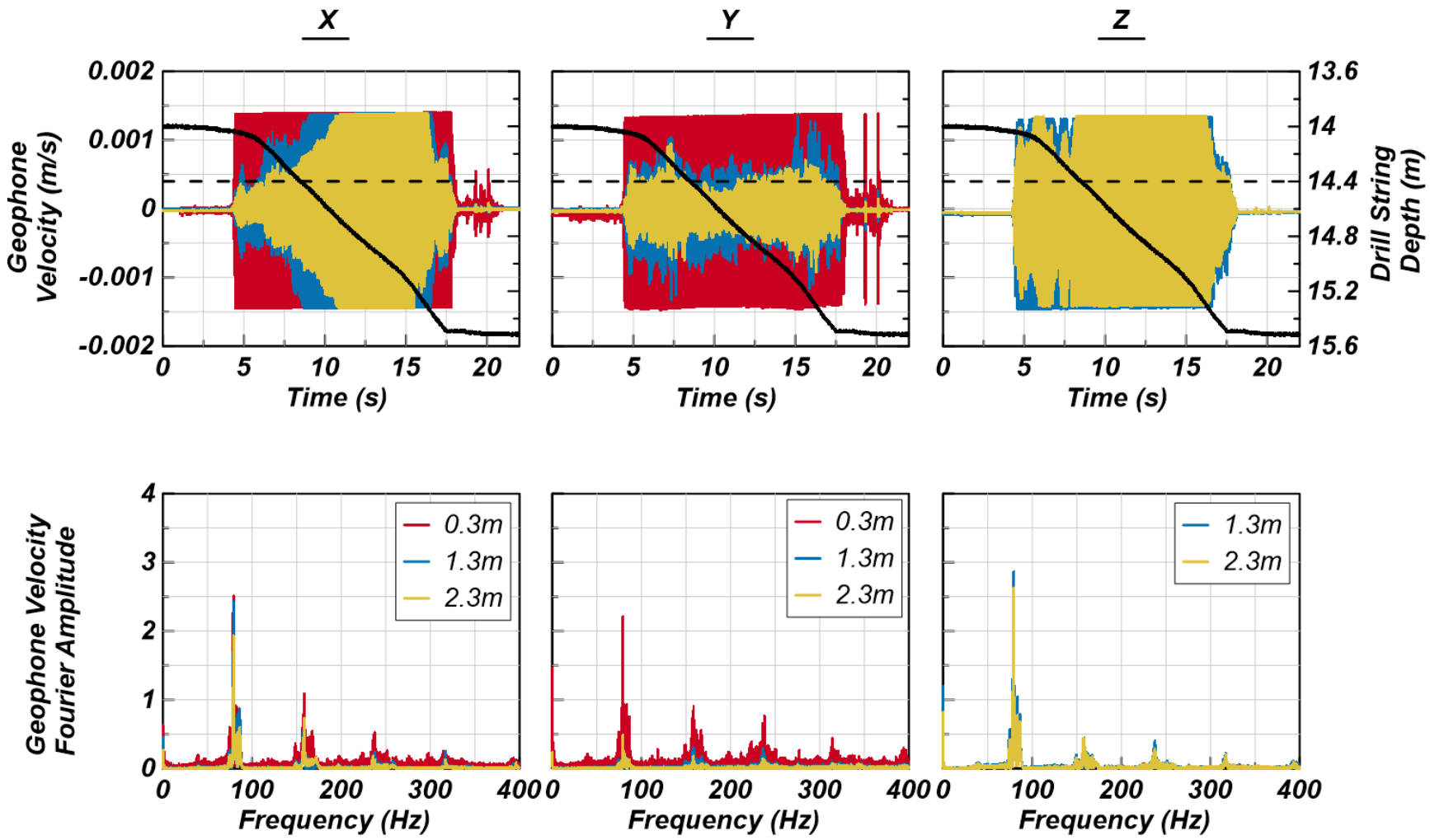

Figure A7 – Phase I velocity time histories and Fourier amplitude spectra recorded during SB2 from 15 to 15.5 m.

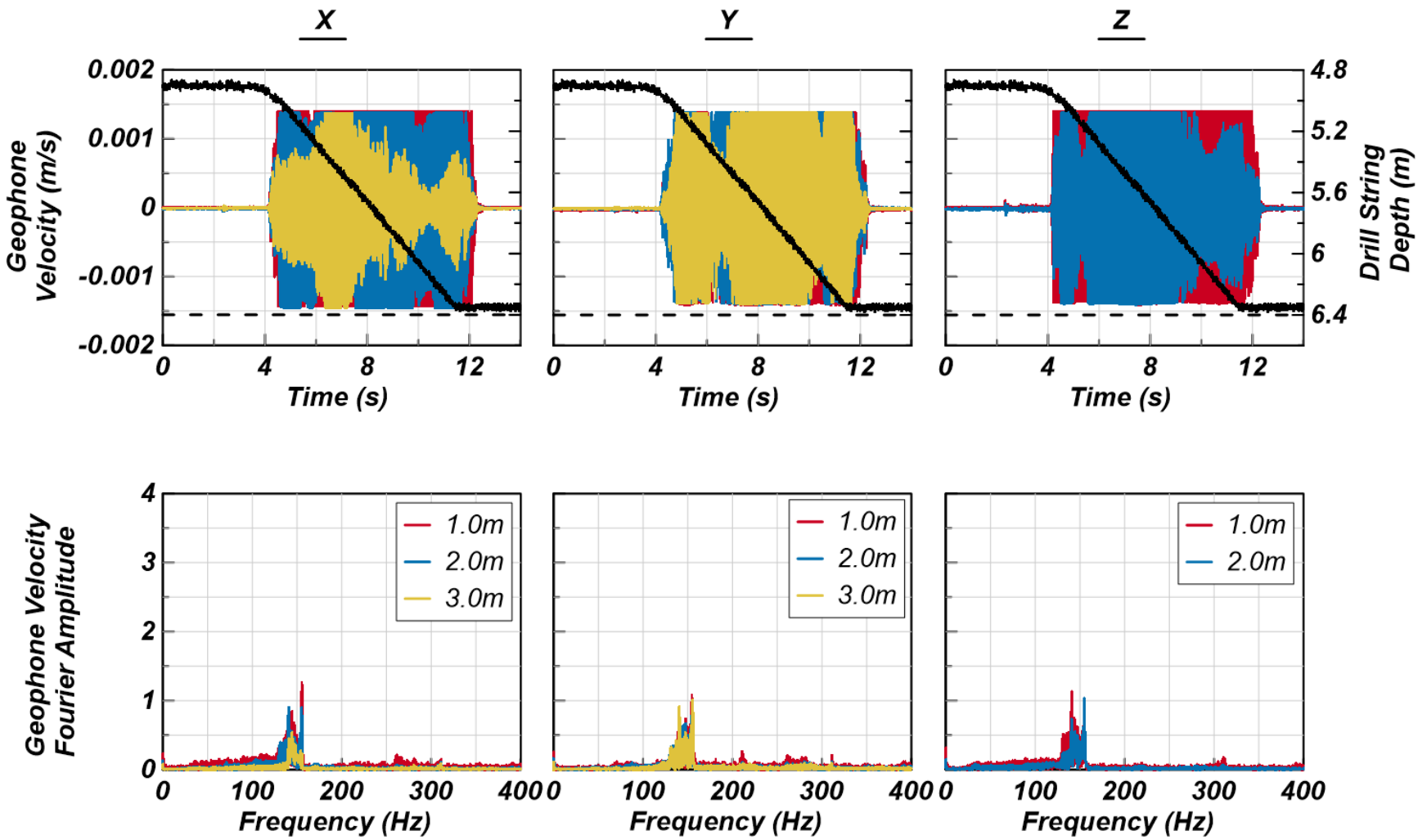

Figure A8 – Phase I velocity time histories and Fourier amplitude spectra recorded during SB3 from 4.9 to 6.4 m.

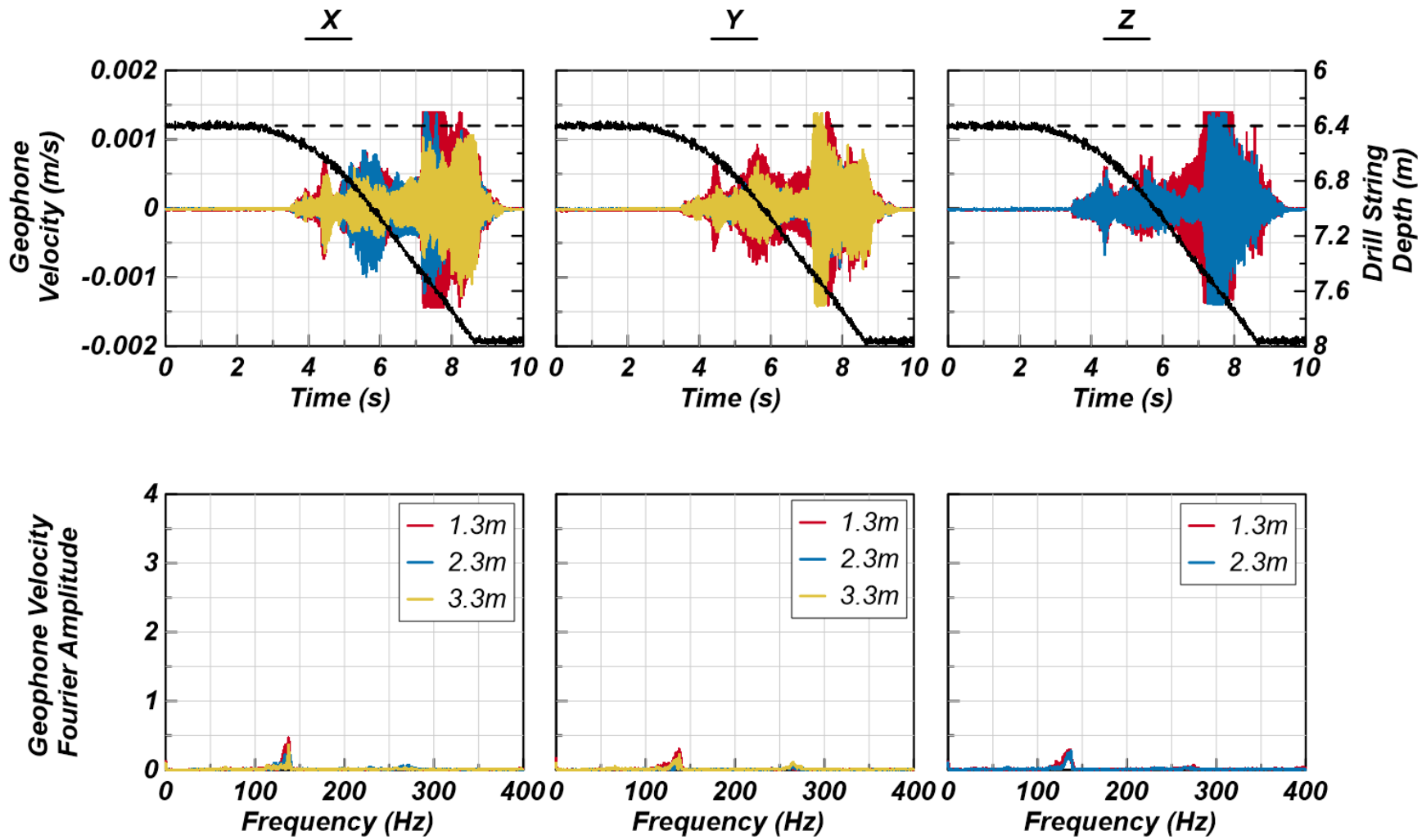

Figure A9 – Phase I velocity time histories and Fourier amplitude spectra recorded during SB3 from 6.4 to 8.0 m.

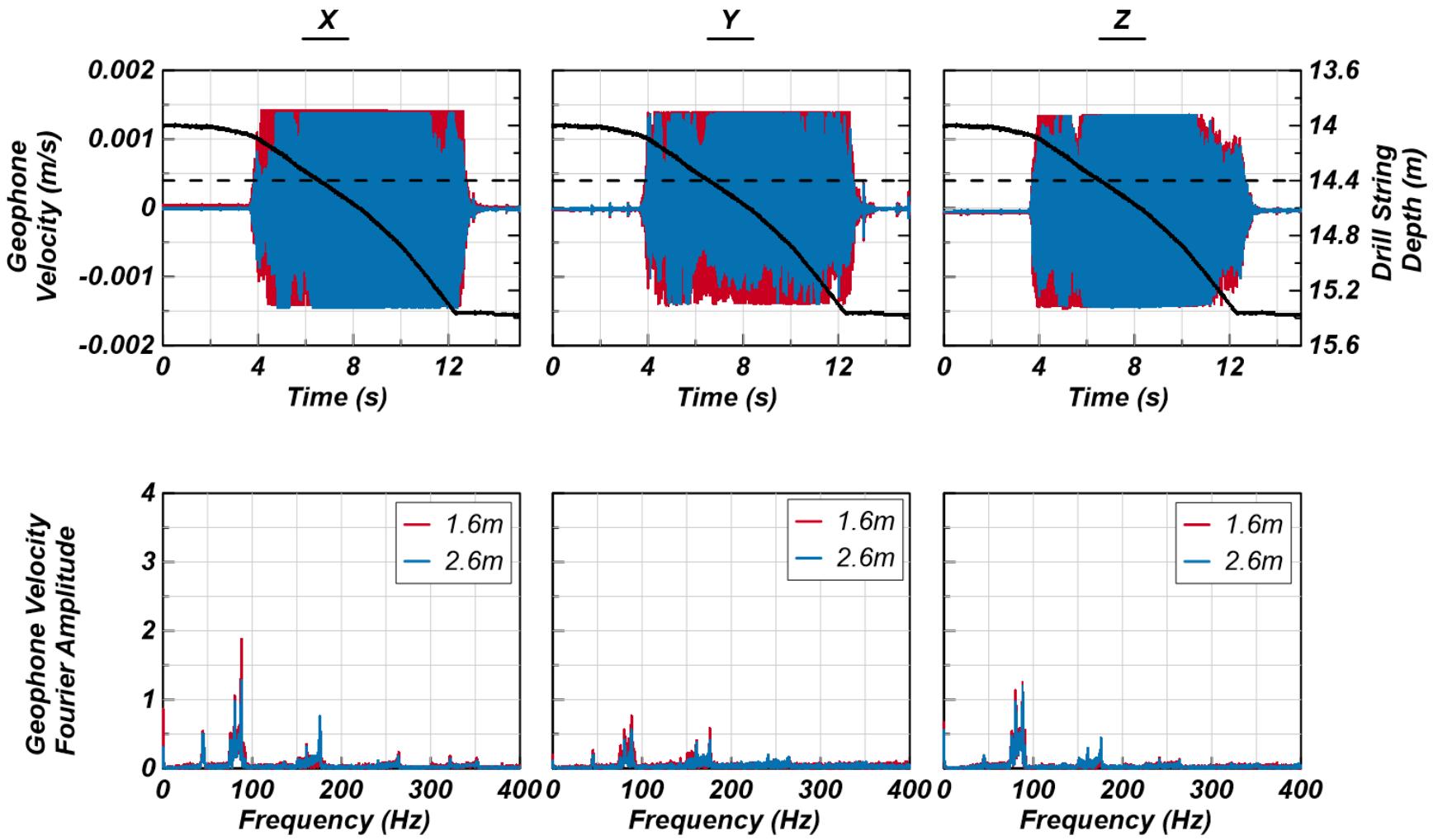

Figure A10 – Phase I velocity time histories and Fourier amplitude spectra recorded during SB3 from 14.0 to 15.4 m.

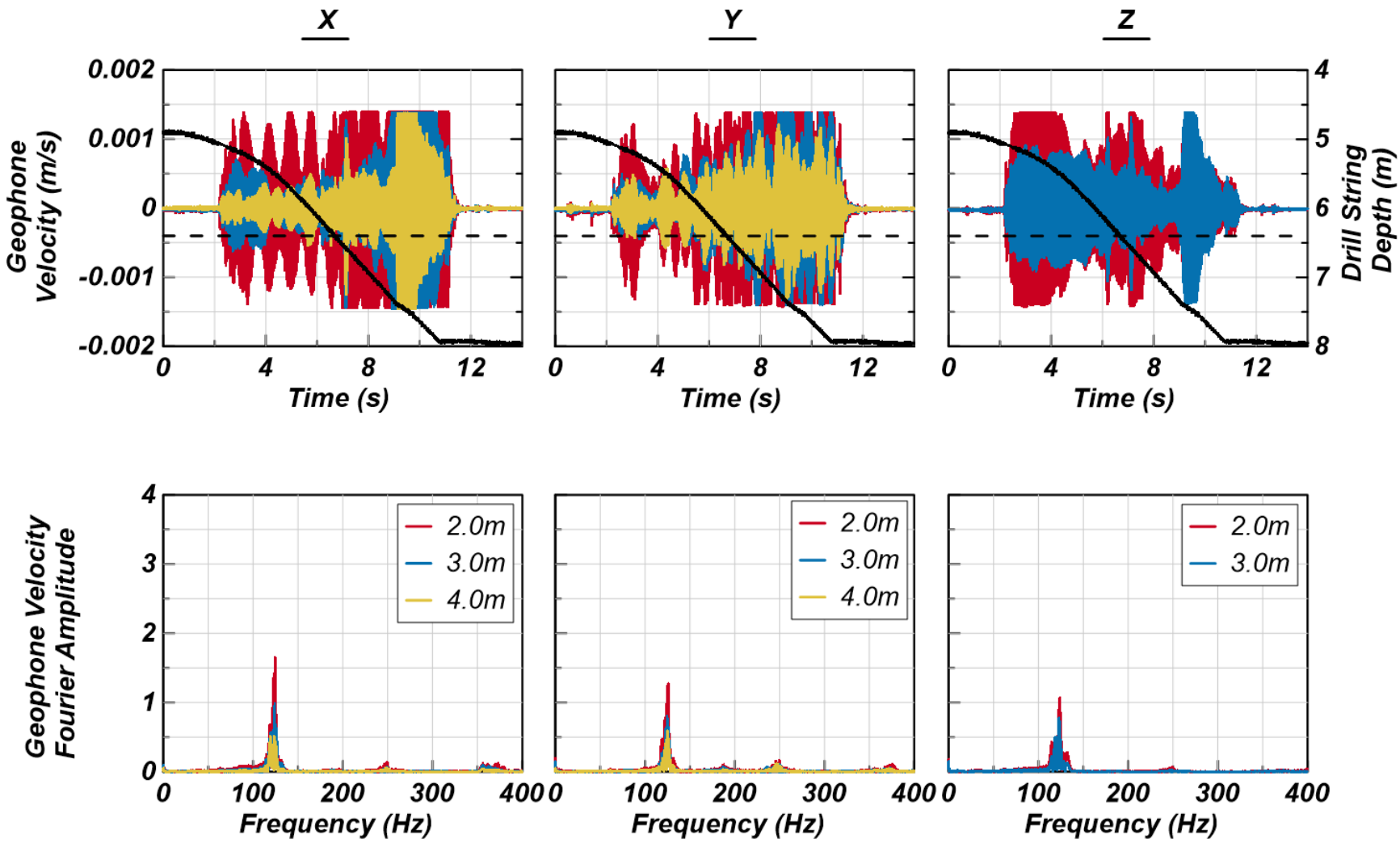

Figure A11 – Phase I velocity time histories and Fourier amplitude spectra recorded during SB4 from 5.0 to 8.0 m.

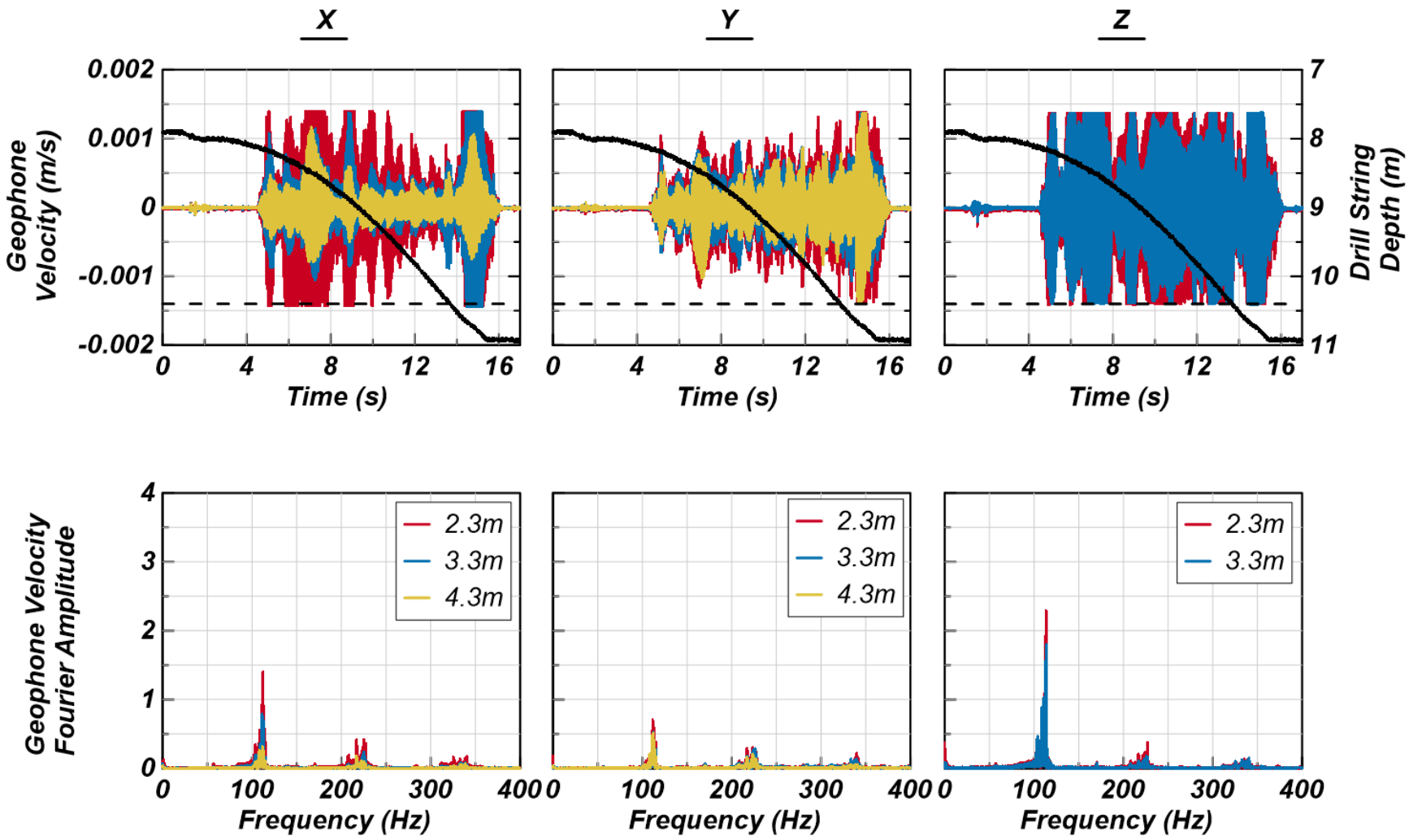

Figure A12 – Phase I velocity time histories and Fourier amplitude spectra recorded during SB4 from 8.0 to 11.0 m.

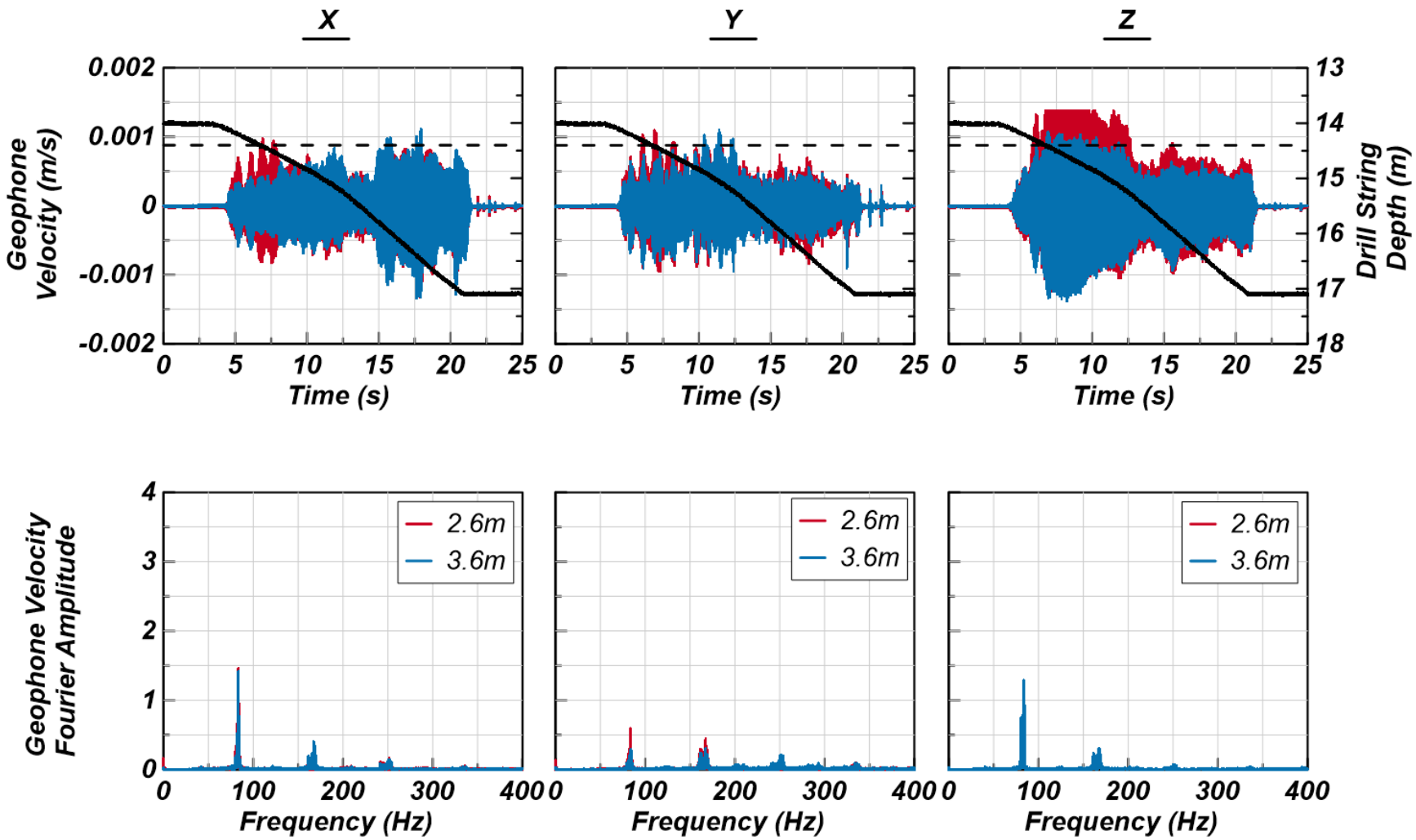

Figure A13 – Phase I velocity time histories and Fourier amplitude spectra recorded during SB4 from 14.0 to 17.0 m.